Weather and Forecasting Challenges in the Pacific Region of the National Weather Service

KEVIN R. KODAMA*

Joint Institute for Marine and Atmospheric Research, Honolulu, Hawaii

STEVEN BUSINGER

Department of Meteorology, University of Hawaii, Honolulu, Hawaii

(Manuscript received 10 April 1997, in final form 2 October 1997)

ABSTRACT

The large area of responsibility covered by the Pacific Region of the National Weather Service provides a unique set of challenges to operational forecasters. Extratropical, subtropical, and tropical meteorological phenomena on a wide range of temporal and spatial scales must be considered on a daily basis. Compounding the problems of forecasting diverse weather for such a large area of responsibility is the fact that the Pacific Ocean is a data-sparse region. Recent improvements in data collection platforms and the continued progress made by researchers have helped increase the understanding of weather throughout the region, ultimately resulting in improved forecast services.

This article provides an overview of some of the weather phenomena encountered in the Pacific Region and helps set the stage for the accompanying articles that focus on specific weather forecasting problems. Some discussion is provided on the impact of the National Weather Service's modernization program on operational forecasting in the region.

1. Introduction

Although it is the smallest of the six administrative regions, the Pacific Region of the National Weather Service (NWS), hereafter the ''Pacific Region,'' covers by far the largest geographic area of responsibility (AOR). Its two forecast offices are responsible for providing weather, marine, and hydrologic forecasts, warnings, and watches to a large portion of the Pacific Ocean. This is an area more than twice the size of the continental United States and includes the State of Hawaii, two U.S. trust territories (Guam and American Samoa), and four foreign countries. These political entities consist of islands and atolls from the Mariana Islands, the Caroline Islands, the Marshall Islands, the Hawaiian Islands, and the Samoa Islands (Fig. 1). The foreign countries, the Commonwealth of the Northern Mariana Islands, the Republic of Palau, the Federated States of Micronesia, and the Republic of the Marshall Islands, are provided weather support under the auspices of the Compact of Free Association with the U.S. government.

Because of its size, the Pacific Region's forecasters are frequently challenged with a wide range of meteorological phenomena that include extratropical, subtropical, and tropical systems. These systems generate the heavy rains, high surf, and strong winds that constitute the region's greatest weather-related hazards and forecast challenges. Complicating the forecast process is the paucity of observational data and the variability introduced by the interactions between the weather systems and terrain that ranges from atolls only a few meters above sea level to large islands with volcanoes reaching up to 4-km elevation.

The threat to life and property from heavy rains and flash floods is particularly significant in the Hawaiian Islands, accounting for most of its damaging weather events with an average of six heavy rain events per year, at least one of which has rainfall greater than 250 mm day^{-1} (Kodama and Barnes 1997). In many of the Hawaiian stream basins, response times to heavy rains are less than 1 h and even as fast as 15 min, making the timely detection of heavy rain extremely important. Adding to the forecast challenge is the fact that flood-producing rains can come solely from warm-top convection, which is not easily detected in satellite imagery. Notable examples include the Oahu New Year's Eve flood (31 December 1987–1 January 1988; Department

*Current affiliation: NOAA, NWS Forecast Office, Honolulu, Hawaii.

Corresponding author address: Kevin Kodama, WSFO Honolulu, 2525 Correa Road, Suite 250, Honolulu, HI 96822.
E-mail: kevin.kodama@noaa.gov

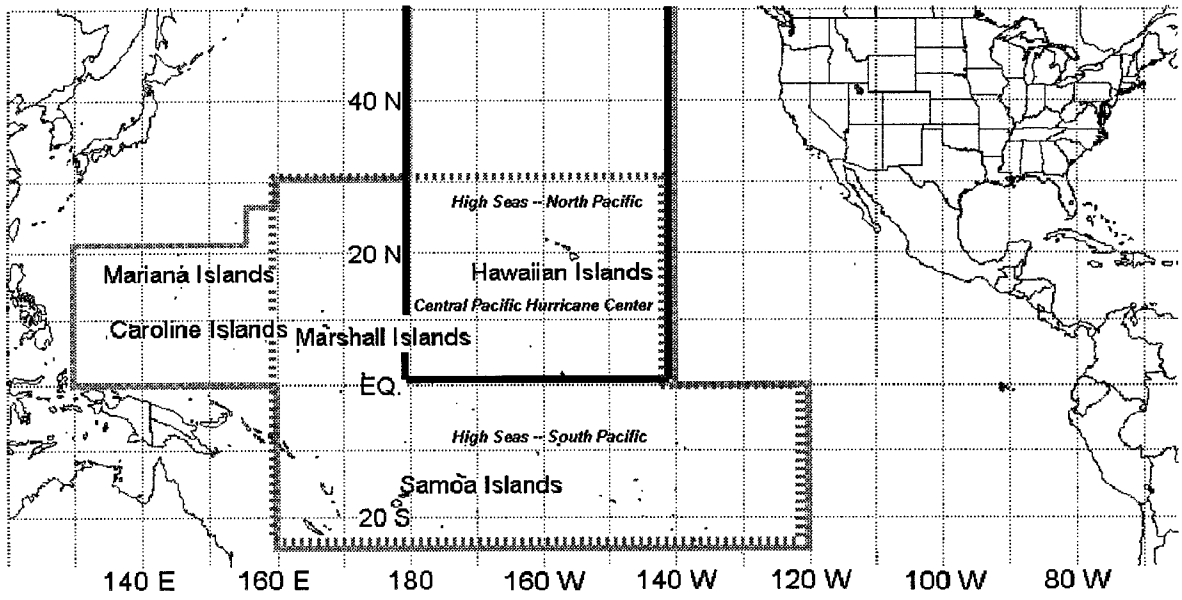

FIG. 1. Map of the Pacific Region's area of responsibility (AOR). The areas covered by the different forecast products are subsets of the entire AOR. For example, the Central Pacific Hurricane Center (area within the bold black line) in Honolulu, Hawaii, issues forecasts, warnings, and advisories for all tropical cyclone activity within the region north of the equator between 180° and 140°W. The area within the dashed gray line is the region covered by the High Seas Forecast, issued by the WSFO Honolulu. Other forecast products include forecasts and advisories for aviation terminals and routes, marine interests in coastal and offshore waters, and public state, zone, and local forecasts.

of Land and Natural Resources 1988) and the February 1979 Hilo, Hawaii, heavy rain event (Cram and Tatum 1979). Both cases exhibit warm-top convection with maximum 24-h rainfall in excess of 585 mm. Cram and Tatum note cloud tops of less than 4 km in the February 1979 case.

High surf accounts for most of the Pacific Region's weather-related fatalities. In the Hawaiian Islands, extratropical cyclones are the most frequent cause of high surf events. Strong, slow-moving storm systems that develop far to the northwest of the islands can generate large swells that produce surf heights in excess of 6 m along north-facing shores. Southern Hemisphere extratropical cyclones that form during the austral winter can also generate Hawaiian south shore surf heights over 3 m. Due to their location, the islands and atolls of Micronesia experience a much higher percentage of high surf events from tropical cyclone activity than is experienced in Hawaii (D. Mundell and J. Pangelinan 1997, personal communication). Low-lying atolls are also vulnerable to inundation from tropical cyclone storm surges and high surf from westerly gales and distant extratropical cyclones. For example, portions of Majuro Atoll, with a maximum elevation of ~4.5 m, have been inundated twice in the last five years.

While not as frequent as heavy rain or high surf events, strong wind events are responsible for most of the Pacific region's weather-related monetary losses. In the Hawaiian Islands, most of the damaging wind events are due to strong extratropical and subtropical cyclones, though strong anticyclones also produce destructive trade wind events. In Micronesia, most of the damaging wind events are due to tropical cyclone activity (K. Waters 1997, personal communication).

This paper provides an overview of some of the meteorological phenomena that Pacific Region forecasters consider in developing forecasts and to discuss some of the impacts of the ongoing NWS modernization and associated restructuring (MAR) program on the region's operations. The articles accompanying this paper examine a few of these issues in greater detail. These include papers on a Hawaiian severe weather event and on the implementation of the National Centers for Environmental Prediction (NCEP) Regional Spectral Model (RSM) for operational forecasting in Hawaii.

2. The large-scale environment

The main components of the general circulation affecting the tropical Pacific are the Hadley circulation and the Walker circulation. The Walker circulation, a term first coined by Bjerknes (1969), is the zonal component and includes several large-scale, thermally direct circulation cells within the equatorial regions of the globe. Normally, the cell over the Pacific contains an ascending branch in the equatorial western Pacific and a descending branch in the eastern Pacific. In the thermally direct Hadley circulation, air rises near the equator and flows poleward aloft. This poleward-moving air is generally subsident and results in a semipermanent anticyclone at the surface in the subtropical latitudes of the northeastern and southeastern Pacific. The anticy-

clones go through an annual migration. For example, the mean January position of the northeast Pacific anticyclone is near 30°N, 130°W, with a subtropical ridge extending southwestward to near 25°N (Fig. 2). By July, the anticyclone has expanded considerably with its center shifted northward to near 35°N, 155°W and the subtropical ridge axis between 30° and 35°N. The flow around these anticyclones results in northeasterly (southeasterly) low-level winds over the tropical North (South) Pacific. Known as the trade winds, this persistent low-level flow regime plays a major role in defining the climatology of the region. Over the Hawaiian Islands, trade winds occur ~70% of the year. A seasonal stratification shows that they are most persistent during the summer months, when trade winds blow on ~90% of the days. During the Hawaiian cool season (October–April), equatorward excursions of extratropical storms may cause a temporary loss of trade wind flow. As a result, the trade wind frequency for Hawaii drops down to ~50% (Schroeder 1993). The annual trade wind frequency in the western North Pacific is similar to Hawaii at ~75%. Unlike Hawaii, however, the trades experienced at locations such as the Mariana Islands are most persistent during the winter months (~90%) and least persistent during the summer (~40%) (NCDC 1996). The summer minimum in trade wind frequency is a result of a monsoon trough that can move over and north of the Mariana Islands during this time of the year causing southwesterlies equatorward of the trough axis.

Convergence of the Northern and Southern Hemispheric trade winds occurs just north of the equator in an area that will be referred to in this paper as the near-equatorial trade wind convergence (NETWC; Ramage 1995). This area is often referred to as the intertropical convergence zone (ITCZ). However, Ramage notes that the term ITCZ suffers from a variety of definitions that can include not only the region of trade wind convergence, but also the monsoon trough, a feature defined by the presence of deep, moist southwesterly flow to the south of the trough axis and known to be a favored region for tropical cyclogenesis. Thus, following the Ramage convention, this paper will use the more specific term of NETWC to distinguish this feature from the monsoon trough. The NETWC migrates following the march of the seasons and reaches its northernmost extent near 10°N during the boreal summer, then pushes southward to roughly 5°N during the boreal winter (Fig. 2). Large-scale ascending motion in this region results in a moist, unstable air mass that is able to support outbreaks of deep convection (Fig. 3).

Areas within the trade wind regime poleward of the NETWC often lie beneath a feature called the trade wind inversion that blocks the development of deep convection (Fig. 3). The height of the inversion gradually increases as one moves away from the center of the subtropical anticyclone toward the equator. Observations show that in the northeast Pacific between 30° and 35°N, inversion heights are near the 1000-m level (Riehl 1954). Around the Hawaiian Islands, the average trade wind inversion base is near the 2300-m level. Although the height of the inversion near Hawaii can vary considerably from day to day, it usually remains between 1500 and 3000 m above sea level (Grindinger 1992). Data suggest that the increase in trade wind inversion height does not continue all the way to the NETWC. In separate experiments, Ramage et al. (1981) and Kloesel and Albrecht (1989) show little change in the height of the trade wind inversion (near 2000 m) between 15°N and the NETWC. Instead, variability presents itself in the frequency of inversion occurrence, with inversions being less frequent near the NETWC.

Another large-scale convergence feature affecting the Pacific region is the South Pacific convergence zone (SPCZ). The SPCZ extends southeastward from New Guinea past the Samoa Islands to approximately 30°S, 140°W and is one of the most persistent and expansive convective cloud bands on earth (Vincent 1994). During the austral summer (Fig. 2, top), the monsoon trough forms the western portion of the SPCZ, while the eastern portion is associated with tropical and extratropical systems (Ramage 1995). In the austral winter (Fig. 2, bottom), the SPCZ lies in a zone of low-level moisture convergence between the western end of the eastern Pacific subtropical anticyclone and southeasterlies from higher latitudes. Active periods of the SPCZ can result in periods of persistent rain and the passage of deep convective systems over the Samoa Islands (Fig. 4). Thus, the islands in the American Samoa group are known for their wet climate, averaging over 3000 mm and 27 thunderstorm days per year at Pago Pago airport. The annual cycle of SPCZ convective activity shows peak intensity during the austral summer.

During the boreal summer months, deep large-scale southwesterlies in the low levels become established over the low latitudes of the western North Pacific due to the eastward expansion of the Asian summer monsoon trough (Lander 1996). Although the western end of the trough is geographically anchored over the Asian continent, its oceanic portion shows considerable variability in its position, shape, and orientation throughout the western North Pacific monsoon season (June through November). The area near the trough axis is noted as a favorable region for the genesis of tropical cyclones and monsoon depressions while the area south of the trough experiences considerable deep convection. Normally, the trough axis extends east-southeastward from south Asia as far as 160°E. On average, the trough takes a temporary southwest–northeast orientation once per year between mid-July and mid-October. This change in orientation is labeled a ''reverse-oriented monsoon trough'' (Lander 1996) and has a significant impact on tropical cyclone tracks in the western North Pacific.

The interannual variability of large-scale patterns is considerable in the Pacific Region, particularly with the pronounced effects of the El Niño phenomenon. A description of the anomalies that accompany an El Niño

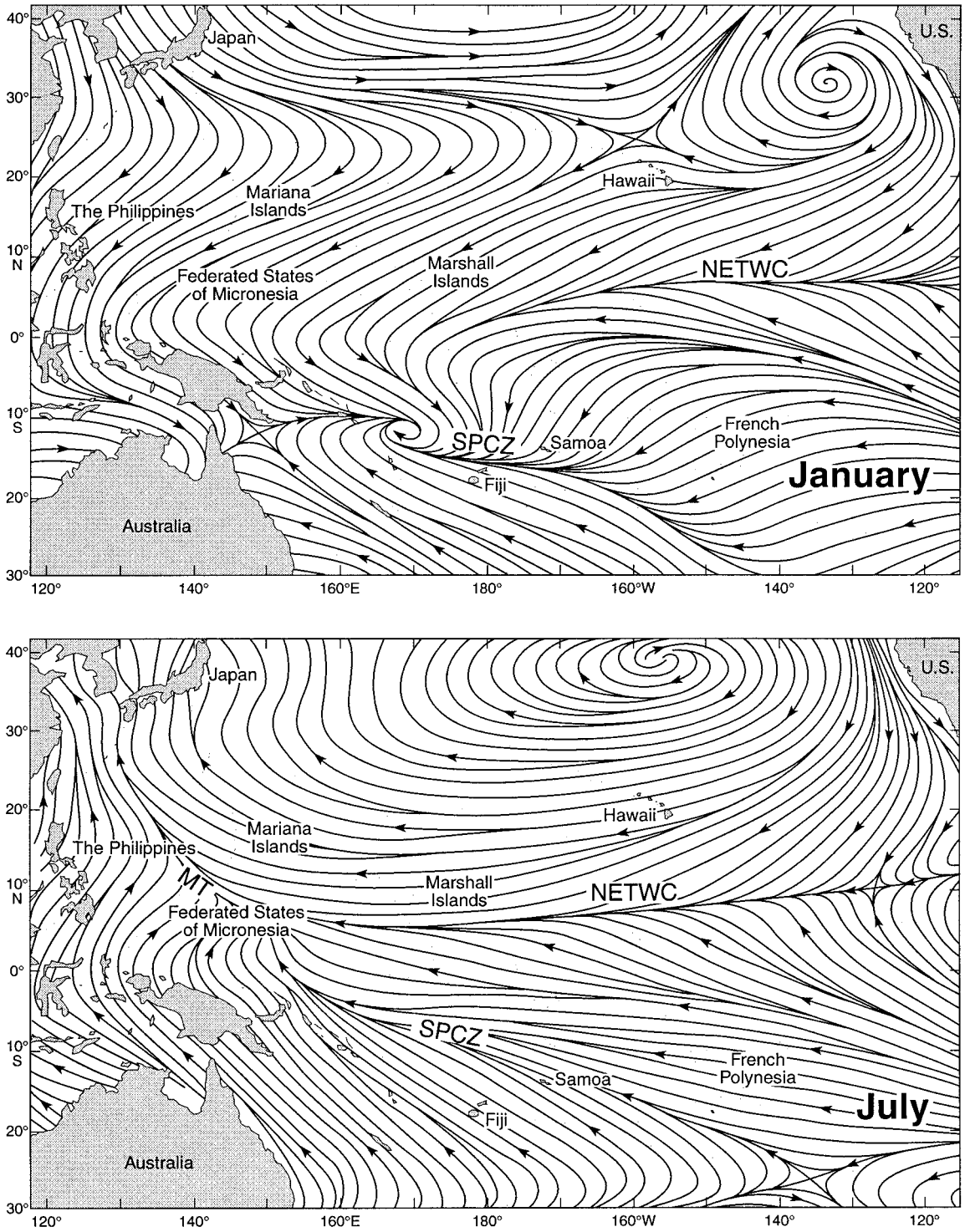

FIG. 2. Streamlines of resultant surface winds over the Pacific for January (top) and July (bottom; after Sadler et al. 1987). Labeled are the near-equatorial trade wind convergence (NETWC), South Pacific convergence zone (SPCZ), and the monsoon trough (MT) in the west Pacific in July.

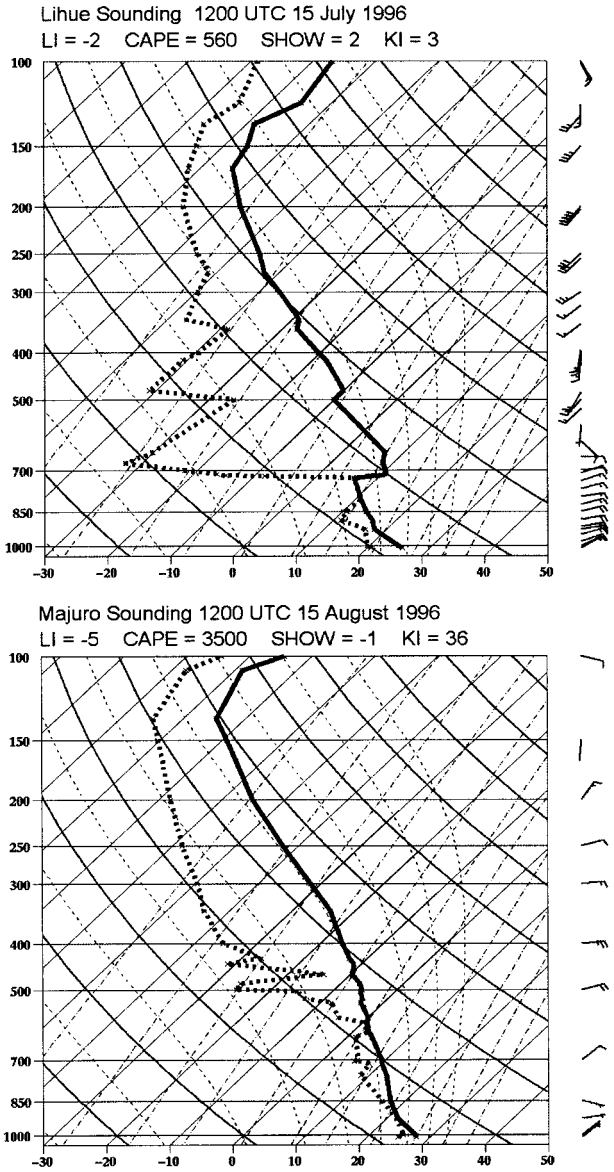

FIG. 3. Skew *T*–log*p* diagrams for (top) 1200 UTC 15 July 1996, Lihue, Hawaii (22°N, 159°W), and (bottom) 1200 UTC 15 August 1996, Majuro Atoll, Republic of the Marshall Islands (7°N, 171°W). Stability indices are listed at the top left of each diagram. LI is the lifted index, CAPE is convective available potential energy, SHOW is the Showalter stability index, and KI is the K index. The Lihue sounding shows a good example of the trade wind inversion (near 720 mb, ~2800 m). The Majuro sounding is an example of atmospheric conditions often found near the NETWC.

are provided by Rasmussen and Carpenter (1982) in a study that composites six events during 1950–76. Summaries of the phenomenon also appear in Philander (1985) and Ramage (1986, 1995). During an El Niño (warm) event, anomalous warm sea surface temperatures occur over the central and eastern equatorial Pacific. Among the atmospheric responses is an eastward shift of the Walker circulation resulting in a significant increase in deep convective activity in the central equatorial Pacific and atmospheric teleconnections extending well into the extratropical regions (Horel and Wallace 1981; Fig. 5). For the islands in the Pacific, one of the more important impacts of El Niño is its influence on rainfall. Many of these islands depend on catchment as the primary source of fresh water. This results in water resource systems that are very sensitive to the significant interannual variability of rainfall. During drought periods on the smaller islands (e.g., Marshall Islands), substantial economic resources are devoted to shipping water for basic needs. Studies of regional rainfall patterns by Ropelewski and Halpert (1987) show that El Niño episodes bring higher than normal amounts of rain to the central equatorial Pacific and lower than normal amounts to the western Pacific and the region around the Hawaiian Islands (Fig. 6). Chu (1995) confirms the findings for the Hawaiian Islands, with a more comprehensive rainfall dataset and through the use of a Monte Carlo simulation technique. Data suggest that during El Niño episodes tropical cyclone activity increases in the central Pacific, which is accustomed to weak and sporadic activity. Further discussion of tropical cyclones is deferred to section 3 of the paper.

The phase opposite of El Niño, called the La Niña, is associated with strong equatorial easterlies, cool central equatorial Pacific sea surface temperatures, and the locus of deep convective activity over the western end of the Pacific (Fig. 5). Ropelewski and Halpert (1989) show that during La Niña, low amounts of rain occur over the central equatorial Pacific, while most of Micronesia, the Hawaiian Islands, the central South Pacific (including the Samoa Islands), and Indonesia receive higher than normal amounts (Fig. 6).

In addition to variability on interannual timescales, intraseasonal variability also occurs. One notable example is the Madden–Julian oscillation (MJO). This feature was first noted by Madden and Julian (1971) who discussed the coherence between surface pressure, zonal winds, and temperatures at several levels with spectral peaks of around 40–50 days (Madden and Julian 1994). Further research showed that the MJO consists of large-scale circulation cells oriented in the equatorial plane that move eastward from the Indian Ocean into the central Pacific. Data suggest that these cells may even propagate around the globe, though in a weaker state east of the central Pacific. Furthermore, evidence suggests that an active MJO phase can stimulate tropical cyclone formation (Nakazawa 1988).

3. Synoptic-scale considerations

Throughout the year, Pacific Region forecasters are challenged by a variety of synoptic-scale systems that can produce heavy rains, strong winds, and high surf. Even blizzard conditions can occur on the higher elevations in the Hawaiian chain during the cool season, adversely impacting astronomical observatories. Im-

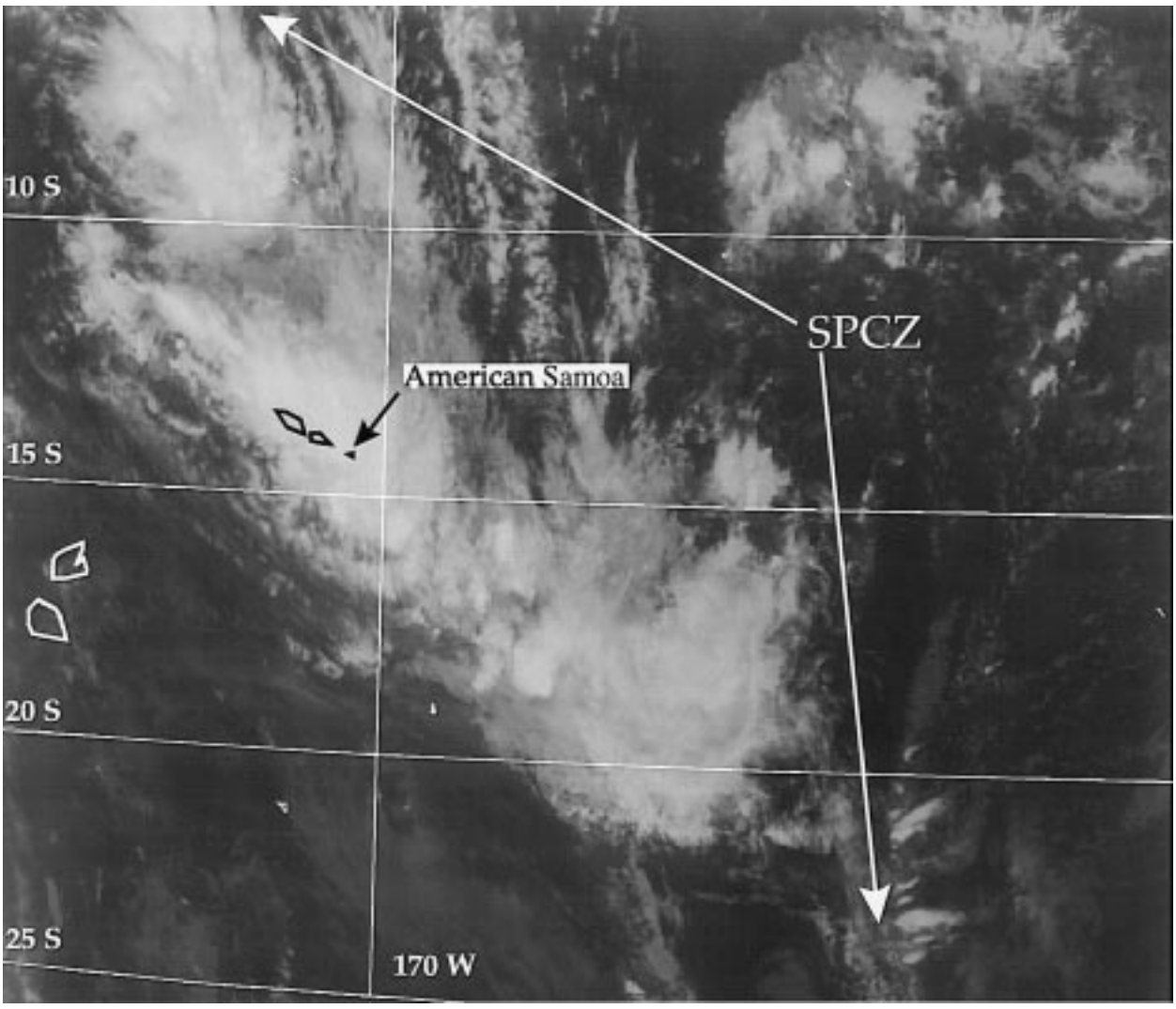

FIG. 4. *GOES*-9 infrared satellite image from 2322 UTC 7 January 1997 showing an active period of the SPCZ affecting the Samoa Islands. This particular convection outbreak dropped 295 mm of rain in a 24-h period at the Pago Pago airport, American Samoa. Two tropical cyclones were also spawned during this SPCZ flare-up.

portant types of synoptic-scale systems include extratropical cyclones, kona storms, upper-tropospheric cold core lows, tropical cyclones, monsoon gyres, monsoon depressions, and westerly wind bursts. Each will be briefly discussed in this section.

a. Extratropical cyclones

In the cool season, extratropical cyclones develop with sufficient strength to push cool air masses with their attendant cold fronts into the subtropical and tropical latitudes of the western and central regions of the Pacific (Fig. 7a). In the Hawaiian Islands, an average of nine cold fronts per year have sufficient strength to pass through the entire island chain (Worthley 1967). Since the cool air mass experiences considerable modification from the relatively warm ocean, a temperature drop at the surface of 4°C with the passage of a cold front is considered to be strong (Levinson 1990). Heavy rains and flash flooding have been associated with cold fronts, the duration of the rains depending, in part, on the propagation speed of the front. Frequently, sufficient frontolysis occurs prior to reaching the Hawaiian Islands so that the only feature that remains of the former cold front is a wind discontinuity with cyclonic shear on its poleward side. This type of feature is known as a shear line. Both cold fronts and shear lines can bring hazardous wind events to the Hawaiian Islands. These wind events can occur in the prefrontal southerlies or the postfrontal northerlies.

b. Kona storms

Strong cool season cyclones can also develop in situ in the subtropical and tropical regions. An ex-

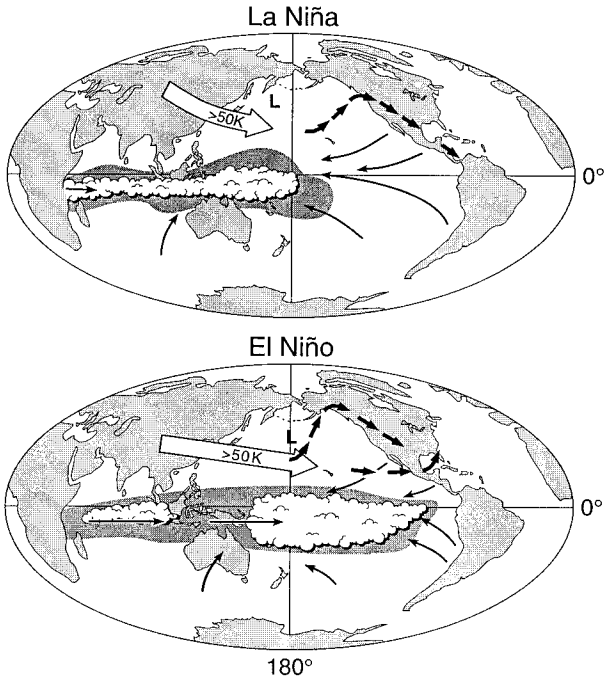

FIG. 5. Conceptual diagram showing the differences between boreal winter conditions in La Niña (top) and El Niño (bottom) years. The Pacific Ocean ''warm pool'' (dark shading) spreads eastward into the central and eastern Pacific, resulting in anomalous convective activity in those regions (indicated by scalloped clouds). El Niño years also show anomalous westerlies in the low-level wind field (thin arrows) and shifts in the upper-level wind patterns (bold arrows).

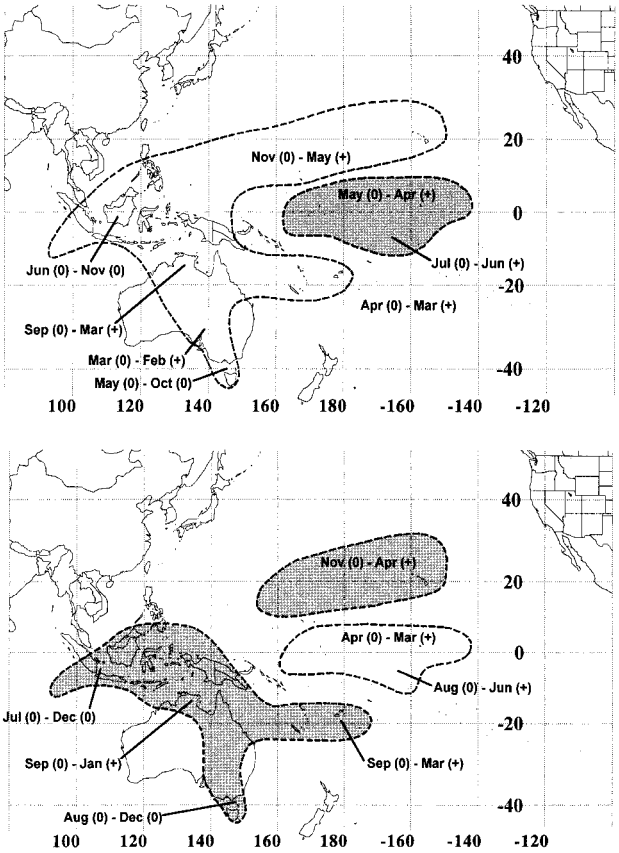

FIG. 6. Map of principal areas (enclosed by dashed lines) of anomalous rainfall in the Pacific Ocean during El Niño (top) and La Niña (bottom). Gray shading shows above-average precipitation, unshaded regions show below-average precipitation. Parenthesized zeros (0) indicate months during an El Niño or La Niña year (Jan–Dec), while parenthesized plus signs (+) indicate months from the year following El Niño or La Niña (adapted from Ropelewski and Halpert 1987, 1989).

ample of this type of system is the subtropical cyclone, also known as the ''kona storm'' (Simpson 1952; Fig. 7b). The Hawaiian word ''kona'' means leeward, in reference to the western slopes of the islands, which are in the lee of the prevailing trade winds. Simpson found that these systems originate from 1) occluded cyclones that become trapped in the low latitudes by blocking from a warm high-pressure cell, or 2) strengthening of an upper-tropospheric disturbance that gradually causes a low-pressure center to develop at the surface. Kona storms generally form in the region bounded by 15°–35°N and 175°E–140°W and move erratically, though with a slow tendency toward the west. These systems are usually very persistent, able to last up to two weeks before being absorbed by a large-amplitude trough in the polar westerlies (Ramage 1962). Kona storms are notorious producers of heavy rain, strong winds, and high surf. The erratic movement and persistence of these systems, both relatively poorly simulated by the operational global forecast models, present a considerable challenge to forecasters who try to predict the onset and cessation of the attendant hazardous weather conditions.

A recent example of a kona storm occurred in November 1995. In this case, the kona storm provided an environment favorable for the development of mesoscale convective systems (MCS) that produced damaging wind gusts ($\sim$40 m s^{-1}) and 24-h rain accumulations $>$250 mm on the island of Kauai. Additional details of both the kona storm and the associated MCS are provided in the accompanying Pacific Region articles by Businger et al.(1998) and Wang et al. (1998).

c. Upper-tropospheric cold core lows

Another synoptic-scale feature that forecasters contend with is the upper-tropospheric cold core low (Fig. 7c). These cold core lows can occur any time of the year but are mainly considered a warm season phenomenon. During the warm season, a train of upper-level cold core lows forms what has become known as the tropical upper-tropospheric trough (TUTT) (Sadler 1967; Whitfield and Lyons 1992). A composite of 117 western North Pacific cold core lows by Kelley and Mock (1982) shows the largest cold

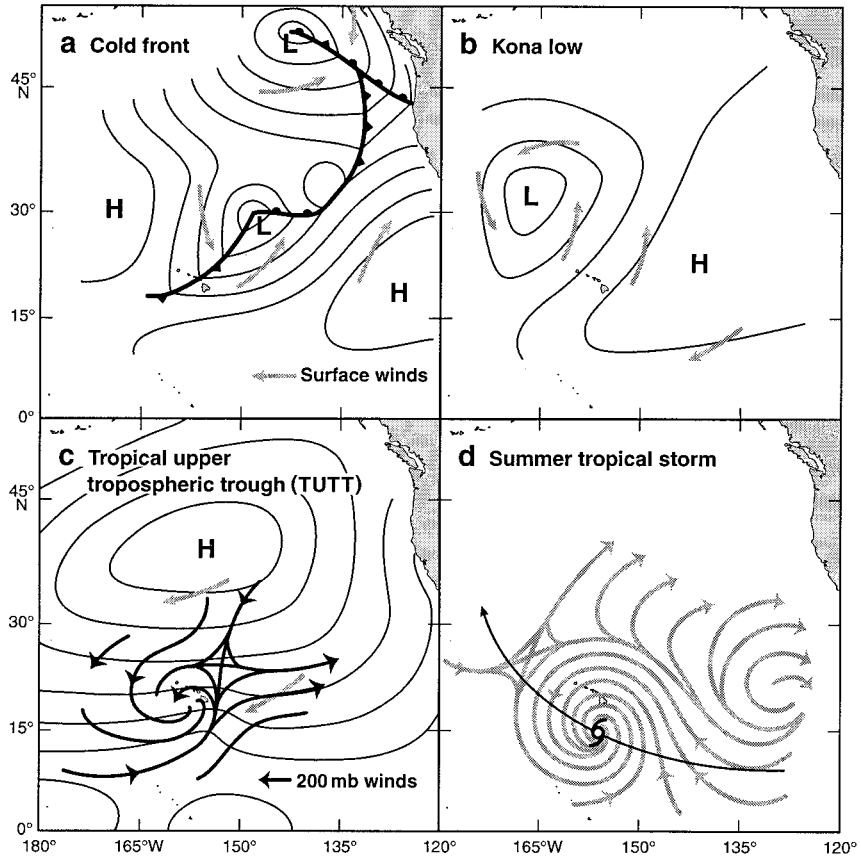

FIG. 7. Conceptual diagram of four types of synoptic-scale systems that affect locations in the Pacific region. Solid lines show idealized surface isobars. Shaded arrows indicate surface flow, bold arrows in (c) indicate 200-mb flow. Solid arrow in (d) indicates the tropical cyclone track.

anomaly at 300 mb, and the strongest circulation around the low at 200 mb. In many cases, the passage of a TUTT over a station results in little noticeable change other than an increase in cirrus. Downward penetration of the low can induce a cyclonic circulation at the surface, resulting in enhanced convection and rain to the east and southeast of the low. Occasionally, short-lived cumulonimbi form in the center of the low (Ramage 1995). Sadler (1976) proposes that the TUTT can play a role in the development of some tropical cyclones by providing an outflow channel aloft that reduces surface pressure via mass conservation arguments. While the TUTT may play a role in certain cases of tropical cyclone formation, it can also play a role in cyclone dissipation. Significant westerlies on the equatorward side of the trough axis overlying low-level easterlies presents an environment that is detrimental to tropical cyclones due to the vertical shear of the horizontal winds. In the central North Pacific, this is an important consideration for forecasters as tropical cyclones frequently meet their demise in this type of environment.

d. Tropical cyclones

Tropical cyclones[1] provide by far the greatest potential for widespread destruction of life and property in the region. Notable examples include Hurricane Iniki (Kauai, September 1992) and Typhoon Omar (Guam, August 1992), with damage estimates around $2 billion and $500 million, respectively. In addition to the well-known destructive strength of its winds, these cyclones can produce significant damage from heavy rains, high surf, storm surges, and tornadoes.

The Pacific Region's AOR lies within the western North Pacific (WNP; west of the date line), central North Pacific (CNP; east of the date line to 140°W longitude),

[1] Definitions of tropical cyclone classes used here are 1) tropical depression: a tropical cyclone with a closed surface circulation and maximum sustained winds (averaged over 1 min period or longer) <17 m s^{-1} (34 kt); 2) tropical storm: a tropical cyclone with maximum sustained winds from 17 to 32 m s^{-1} (34–63 kt); 3) hurricane/typhoon: a tropical cyclone with maximum sustained winds ≥ 33 m s^{-1} (64 kt).

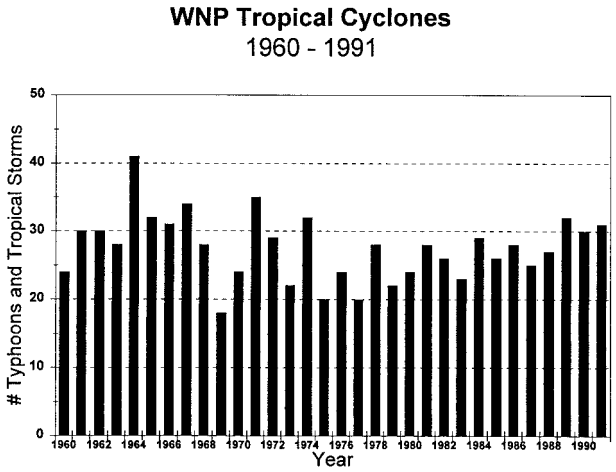

FIG. 8. Number of western North Pacific (WNP) tropical storms and typhoons occurring from March through January of each year for the period 1960–91 (data from Lander 1994).

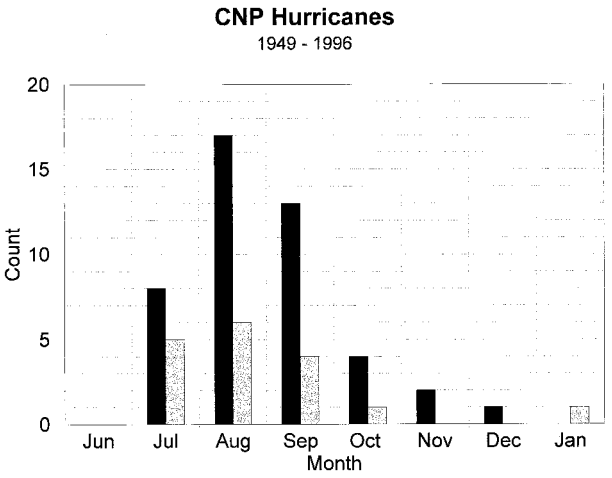

FIG. 9. Histogram of central North Pacific (CNP) hurricanes for the period 1949–96. Black bars are for hurricanes ≥category 1 (maximum sustained winds ≥64 kt, or 33 m s^{-1}). Light gray bars are for hurricanes ≥category 3 (maximum sustained winds ≥96 kt, or 50 m s^{-1}). Hurricane occurrence from January through June is extremely rare in the central Pacific.

and western South Pacific (WSP) tropical cyclone basins. Tropical cyclone formation bulletins and track forecasts for the WNP and WSP (west of 180° longitude) basins are provided by the Department of Defense's Joint Typhoon Warning Center (JTWC) (Guard et al. 1992). Track forecasts for the WSP basin east of 180° longitude are the responsibility of the Fiji Meteorological Service. Based on these forecast bulletins, the NWS generates and disseminates public warnings and advisories for locations within the Pacific Region's AOR. The Pacific Region's Central Pacific Hurricane Center (CPHC), located at the NWS Forecast Office (WSFO) in Honolulu, Hawaii, is responsible for all formation and track forecasts, as well as all public warnings and advisories for the CNP.

The WNP basin is the most active tropical cyclone basin in the world with an annual average of 28 storms at tropical storm strength or greater (Lander 1994; Fig. 8). Cyclone activity can occur in the WNP any time of the year, though the monthly frequency exhibits a strong peak in August. Since the most active cyclogenesis region in this basin is within the area bounded by 5°–20°N and 130°–160°E, the islands of Micronesia are threatened by tropical cyclones several times per year on average. Lander (1996) shows that 58% of the WNP basin tropical cyclones (1978–94) initially move toward the west and either continue straight into the Philippines and Southeast Asia regions (33%) or later recurve toward the northeast (25%). A significant number (23%) have north-oriented tracks. These north-oriented tracks are mainly associated with the occurrence of the aforementioned reverse-oriented monsoon trough.

The WSP basin is the second most active in the world, experiencing an average of 16 tropical cyclones (tropical storm strength or greater) per year (Gray 1985). These systems can form near the SPCZ and sometimes impact the Samoa Islands. Like the WNP, the WSP basin experiences a long tropical cyclone season, peaking during the austral summer months of January and February. The WSP cyclones, unlike those in the WNP and CNP basins, often move with an eastward component with a relatively fast median speed of 9 m s^{-1} (Holland 1984). This movement and speed is attributed to the occurrence of these cyclones poleward of the subtropical ridge, thus placing them within a westerly current.

In the CNP basin, the tropical cyclone frequency is much less, with an annual average of 3.5 cyclones with tropical storm intensity or greater (Shaw 1981). Basin activity is most frequent in the late summer. Activity outside of the tropical cyclone season (June–November) is rare (Fig. 9). Most of the tropical cyclones (~70%) that occur in the CNP form and intensify in the eastern North Pacific (ENP) just to the west of Central America. In these cases the storms persist long enough to travel more than 3000 km across 140°W into the CNP. In most cases, cyclones that move in from the east are past the peak of their life cycle and are weakening. There are many instances where systems from the ENP dissipate and move into the Hawaiian Islands with the trade wind flow. One causative mechanism for this dissipation is the presence of unfavorable vertical shear of the horizontal wind in the central Pacific, though cooler sea surface temperatures may also play a role. While these dissipated systems are not a wind or high surf/storm surge threat, they can still be significant rain producers.

Most of the tropical cyclones that form in or move into the CNP pass south of the Hawaiian Islands (Fig. 10). Occasionally, the presence of a trough in the westerlies to the west of the Hawaiian Islands can result in the turning of the storm toward the north or northeast, thus threatening the island chain. During this type of situation, forecasters are confronted with the problem

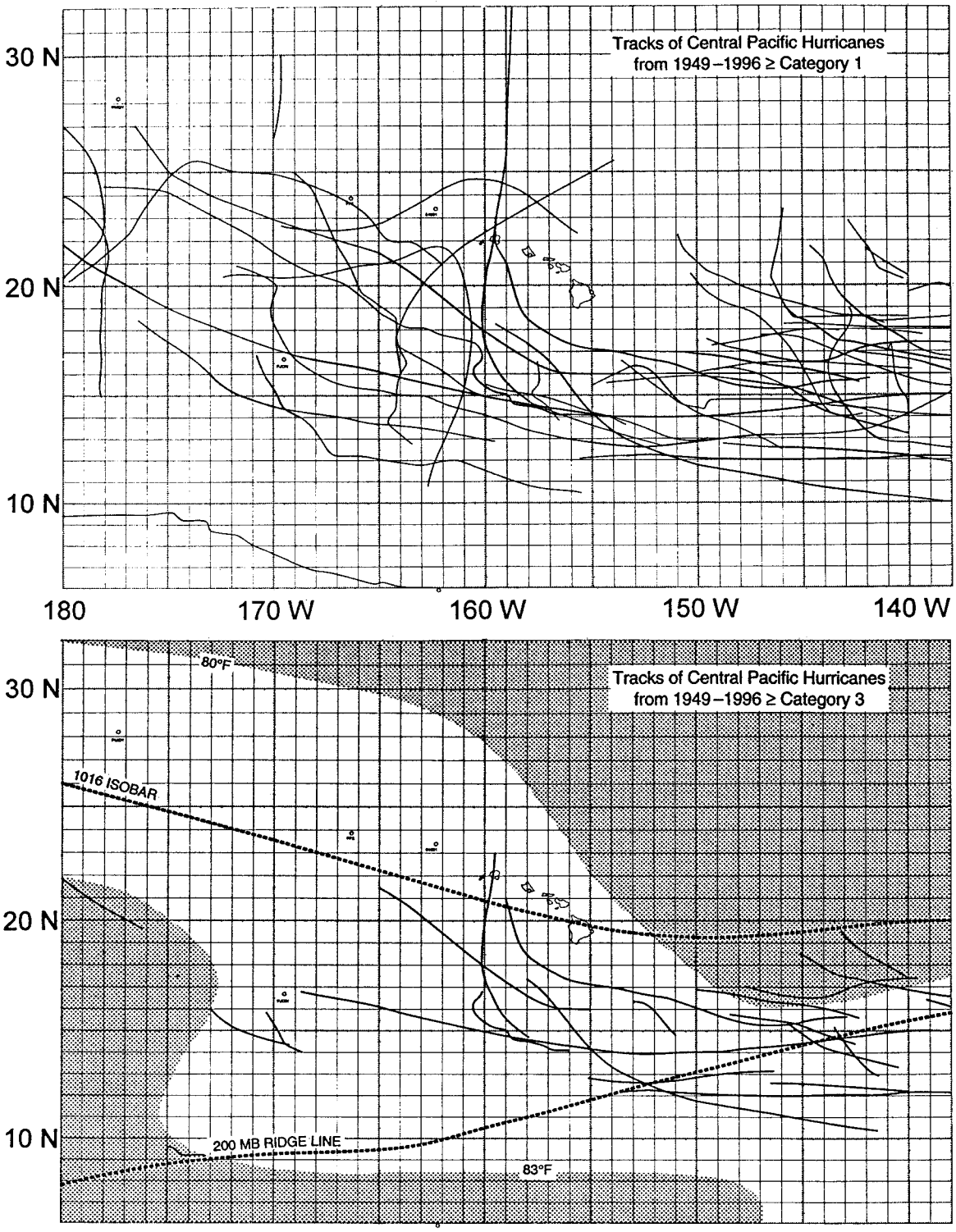

FIG. 10. Central Pacific hurricane tracks from 1949 through 1996 for (upper) ≥category 1 (maximum sustained winds ≥64 kt, or 33 m s^{-1}), and (lower) ≥category 3 (maximum sustained winds ≥96 kt, or 50 m s^{-1}). Also shown are the August mean positions of >80°F and <83°F water (unshaded region), mean 1016-mb isobar (labeled heavy dashed line), and the mean ridge position at the 200-mb level (labeled heavy dashed line), which divides westerly and easterly airstreams aloft.

of deciding what type of influence the trough in the westerlies will have on the cyclone. Will the cyclone indeed turn toward the islands, maintain its intensity and westward motion, or be sheared off and dissipate? Hurricane Iniki in 1992 and Hurricane Emilia in 1994 provide contrasting examples. Hurricane Iniki was an example of a turning situation, having moved westward to the south of the island chain before the influence of a cutoff low pressure system to the west of the islands resulted in a north-oriented track over the island of Kauai (Chun et al. 1993). During Hurricane Emilia, the trough in the westerlies was confined primarily to the upper troposphere. This caused an environment with detrimental vertical shear of the horizontal winds, with upper-level westerlies and low-level easterlies. Therefore, rather than turning northward after passing south of the Hawaiian Islands, Hurricane Emilia rapidly dissipated, its remains moving toward the west in the low-level trade wind flow (Garza et al. 1995).

Due to their significant effects on the wind and sea surface temperature distributions across the tropical Pacific, there is evidence that El Niño events affect tropical cyclone activity in the Pacific Region. In the WNP, the occurrence of El Niño has no relationship to the total number of tropical cyclones that form (Lander 1994). However, there is an eastward shift of the WNP cyclogenesis region, presumably in association with the eastward spreading of warm equatorial sea surface temperatures and the eastward extension of the monsoon trough during El Niño events. There is also a tendency for more tropical cyclones to form in or move into the CNP. Data from a study of the interannual variability of CNP tropical cyclones (Schroeder and Yu 1995) show that the three most active tropical cyclone years since 1970 (when satellite intensity estimates became available) correspond to the occurrence of an El Niño event. The anomalous cyclone activity includes not only a larger number of storms, but also activity outside the normal tropical cyclone season. Recent examples include Hurricane Ekeka (January–February 1992) and Tropical Storm Hali (March 1992) that formed during the 1991–92 El Niño event. In addition to warm SST anomalies in the equatorial central Pacific, Schroeder and Yu cite enhanced low-latitude cyclonic shear zones due to an anomalous eastward extension of the monsoon trough as a factor contributing toward increased CNP tropical cyclone activity during El Niños.

For the WSP basin, there is a tendency for the zone of tropical cyclone activity to shift toward the east, causing an increase in activity near the Samoa Islands. A notable example of the effect of El Niño on WSP tropical cyclone formation is the 1982–83 El Niño event. From December 1982 through May 1983, 11 tropical cyclones formed east of 165°W, with five moving within 500 km of Tahiti. Prior to this, only nine tropical cyclones moved within the same distance of Tahiti during the previous 44 years (Sadler 1984).

e. Monsoon depressions and gyres

In addition to tropical cyclones, the western North Pacific monsoon regime can generate monsoon depressions and monsoon gyres that can have important effects on Pacific region interests. Monsoon depressions form within the monsoon trough and last roughly three to four days (Ramage 1995). Operationally, western North Pacific monsoon depressions are identified based on the following criteria (JTWC 1993): 1) outer most closed isobar diameter on the order of 1000 km, 2) loosely organized cluster of deep convective elements, 3) low-level wind featuring a 200-km diameter light-wind core that may be partially surrounded by a band of gale-force winds (>17 m s^{-1}), and 4) lack of a distinct cloud system center. Many of these systems eventually develop persistent deep core convection and become tropical cyclones (e.g., Harr et al. 1996). This is in contrast to monsoon depressions that form in the Bay of Bengal monsoon trough, which do go through tropical cyclogenesis (Ramage 1971). Due to the strength of its circulation and considerable amounts of deep convection, a monsoon depression can cause widespread weather-related problems due to strong winds, heavy rains, and high surf.

Another western North Pacific monsoonal system is the monsoon gyre (Lander 1994). Occurring approximately once every two years during July through early September, Lander characterizes a monsoon gyre as a large, nearly circular cyclonic vortex with a diameter on the order of 2500 km and a duration of 2–3 weeks. The gyre is separated from the Asian monsoon trough by a north–south-oriented pressure ridge and features a persistent band of deep convection along the periphery of the gyre's southeastern quadrant. Onset of a monsoon gyre also results in a period of increased tropical cyclone activity. These cyclones usually have atypical tracks and appear to develop in two modes; very small systems along the peripheral deep convection band of the gyre, and very large systems as the monsoon gyre itself intensifies and develops into a tropical cyclone.

f. Westerly wind bursts

Observational data from ships and island-based stations have shown that the equatorial western and central Pacific sometimes experience ''bursts'' of westerly winds that replace the normal easterlies and persist for a few days or up to three weeks (Luther et al. 1983). A case study of a May 1982 westerly wind burst by Chu and Frederick (1990) shows winds as strong as 10 m s^{-1} during an episode that lasted 11 days. They also point out that bursts of gale-force intensity have been observed (20 m s^{-1} during a May 1972 event). The exact origins of this phenomenon are unclear, though some investigators (e.g., Murakami and Sumathipala 1989; Chu and Frederick 1990) suggest a midlatitude forcing. Research interest in westerly wind bursts has developed

in recent years with a focus on its ability to force equatorial Kelvin waves that may trigger and sustain El Niño events (e.g., Luther et al. 1983; Lukas et al. 1984). In addition to the generation of Kelvin waves, westerly wind bursts are associated with a significant increase in equatorial deep convection and have been tied to the formation of tropical cyclone ''twins'' that are nearly symmetric with respect to the equator (Keen 1982; Lander 1990). In Lander (1990), surface and satellite observations suggest that the genesis of tropical cyclone twins follows the formation of a strong westerly wind burst and extensive equatorial convection.

4. Mesoscale considerations

Although the synoptic-scale environment determines the larger-scale weather pattern, meteorological impacts to the public are often the result of phenomena that are organized on the mesoscale. For the Pacific Region, these phenomena include tropical disturbances, trade wind disturbances, and MCSs or cloud clusters, as well as orographic and diurnal influences. This section will cover some of the important mesoscale features that play a role in shaping weather in the Pacific Region.

a. Mesoscale convective systems

On any day, satellite imagery will reveal several regions containing deep convective activity across the Pacific (see example in Fig. 4). This convection occurs on a range of spatial and temporal scales, from isolated cumulonimbi with life cycles less than an hour, to large, organized MCSs with upper-level cloud shields occupying several thousand square kilometers and life cycles of several days. These MCSs can be loosely categorized as squall lines or the more frequently observed nonsquall systems (e.g., Houze and Betts 1981; Cotton and Anthes 1989), though many MCSs also fulfill the satellite-based criteria for mesoscale convective complexes (MCCs; Maddox 1980). A study by Miller and Fritsch (1991) of western Pacific MCCs indicates that these systems are common (206 in 3 yr) and exhibit many of the same characteristics as those observed in the Americas.

Tropical squall line MCSs have been defined as disturbances consisting of an active linear deep convection region along the leading edge and a trailing (usually) stratiform region (Houze 1977; Zipser 1977). Squall lines tend to move relatively fast with documented examples of tropical Pacific squall lines showing speeds of 15 m s^{-1} (Zipser 1969) and 12 m s^{-1} (Jorgensen et al. 1997). In addition, orientation of the convective line tends to be perpendicular to the environmental vertical shear of the horizontal wind (Barnes and Sieckman 1984). In general, front-to-rear system-relative flow exists at all levels ahead of the system's leading edge and into the upper-levels of the stratiform region. Rear-to-front flow also exists in the midlevels of the stratiform region. The convective region consists of updrafts and downdrafts with vertical motion magnitudes on the order of several meters per second (e.g., LeMone and Zipser 1980), intense rain, and a gust front, which are attributed to the outflow of evaporation-cooled downdraft air that helps propagate the system. The convective downdraft air also produces a dome of cool air that can stabilize the boundary layer of the affected region.

The trailing stratiform region also exhibits levels of ascent and descent, but is spread over a much larger area with vertical motions on the order of several centimeters per second (e.g., Zipser 1977). While the convective region contains more vigorous motions and more intense precipitation, the stratiform region can account for nearly half of the total rain from the system (Houze 1977; Gamache and Houze 1983). Midtropospheric mesoscale cyclonic vortices can also develop in this region and recent research suggests that these vortices can serve as potential tropical cyclone triggers (Zhang and Fritsch 1987; Miller and Fritsch 1991).

Like the squall-line MCSs, the nonsquall system also consists of convective and stratiform regions, both with ascending and descending components, as well as convective outflows, and front-to-rear system-relative flow (Zipser et al. 1981). However, unlike the distinct precipitation structure of squall lines, the slower-moving nonsquall systems can include several mesoscale precipitation features within one system with a variety of configurations (Leary and Houze 1979). In addition, Barnes and Sieckman (1984) found that the convective line orientation in nonsquall systems is parallel to the environmental vertical shear of the horizontal wind and possesses a weaker equivalent potential temperature minimum near the midlevels of the troposphere.

Forecasting deep convection for the tropical Pacific presents a considerable challenge to the Pacific Region's meteorologists. Large regions of the tropical Pacific are conditionally unstable on any given day and the use of traditional stability indices, such as convective available potential energy (CAPE) and the lifted index, often fail to provide meaningful assistance. In addition, the lack of sufficient surface and upper-air observations hinders attempts to define the stability or the potential trigger mechanisms such as mesoscale convergence zones and vortices. Thus, forecasters depend heavily on satellite imagery to locate large-scale convergence features such as the NETWC and the monsoon trough, as well as the application of conceptual models for synoptic-scale systems to help forecast areas of deep convection. Subtropical locales under the influence of the quasi-permanent Pacific highs, such as the Hawaiian Islands, are much more stable, being frequently under a trade wind inversion. In these areas, forecasters look for synoptic-scale systems (e.g., the kona storm) that can provide sufficient large-scale rising motion to eliminate the subsidence and help facilitate the formation of deep convection.

Pacific Region forecasters must also be aware of

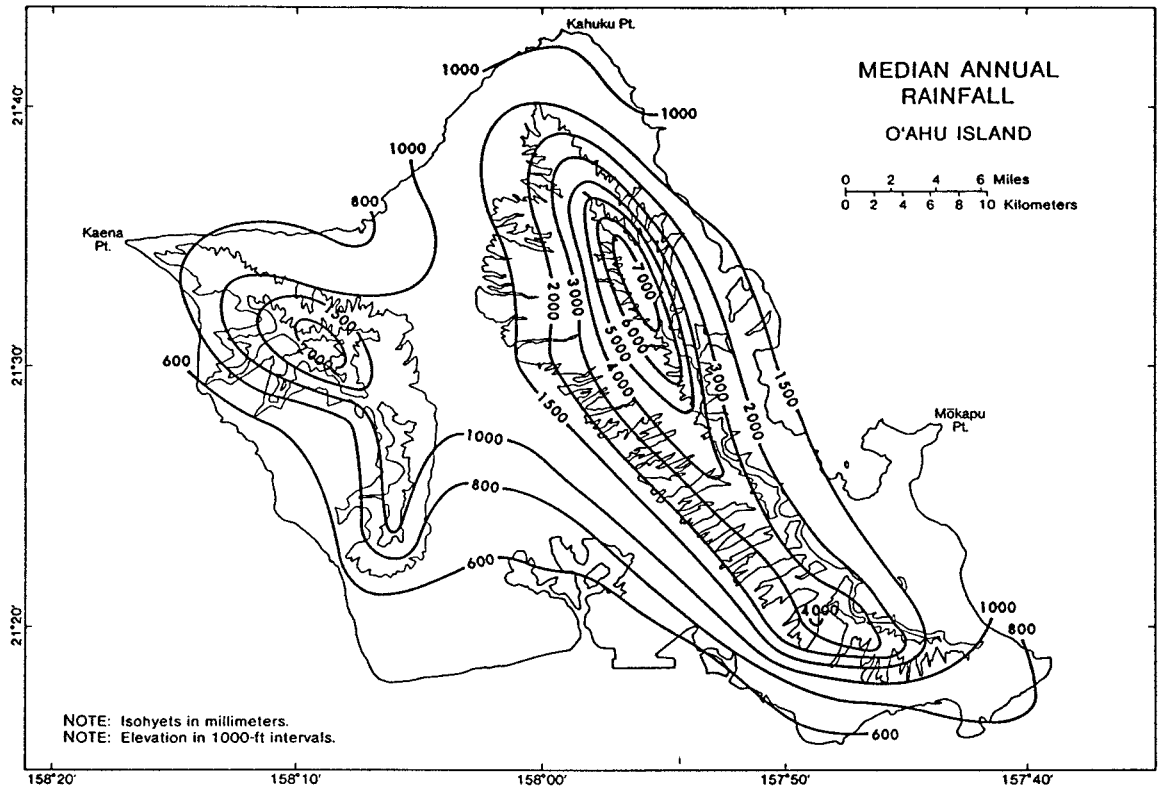

FIG. 11. Median annual rainfall map for the island of Oahu in the Hawaiian Islands. Isohyets are in mm. Note large rainfall gradients (from Giambelluca et al. 1986).

mesoscale systems that can be embedded within trade wind flow that contains limited ambient CAPE. These trade wind disturbances are less obvious in the satellite imagery than cold-topped thunderstorms and appear as warm-topped bands or clusters of open-cell cumuliform cloudiness (Larson 1976). These systems bring periods of enhanced trade wind showers, especially to the windward sides of the affected islands. The passage of two trade wind disturbances near the island of Hawaii during the recent Hawaiian Rainband Project allowed for an examination of these disturbances using aircraft and land-based dual-Doppler radar data. Based on an analysis of both systems, Raymond and Lewis (1995) hypothesized that the mesoscale circulation was driven by localized gradients in the boundary layer equivalent potential temperature field. The radar data also indicated cyclonic rotation in the disturbance, which was attributed to the stretching of absolute vorticity by upward motion.

b. Orographic effects

For the larger mountainous islands, such as those in the Hawaiian chain, orographic effects dominate the local weather regime, having a significant impact on the temporal and spatial rainfall distribution and wind flow patterns. Over the open ocean within the trade wind belt, annual rainfall is low. Dorman and Bourke (1979) estimate the average annual rainfall in the vicinity of the Hawaiian Islands to be ~700 mm. Using modifications of a similar methodology, Elliot and Reed (1984) obtained an estimate of ~550 mm near the Hawaiian Islands. In both studies, horizontal gradients of rainfall were very weak. In contrast, rainfall maps for the Hawaiian Islands (e.g., Giambelluca et al. 1986) show large horizontal gradients and annual amounts in some locations that are more than an order of magnitude greater than the open ocean estimates, due largely to the effects of the island orography on the moist trade wind flow. For those mountain peaks below the average trade wind inversion base (e.g., Ko'olau Range along east Oahu, maximum elevation 960 m; see Fig. 11), rainfall maxima occur near or just downstream (relative to trade wind flow) of the summits. In contrast, mountain peaks that penetrate the trade wind inversion (e.g., Haleakala, elevation 3055 m) have rainfall maxima over the upslope regions, but at an elevation below the average trade wind inversion height.

Wind flow patterns over and near the islands are also strongly influenced by the orography. By using a dimensionless parameter called the Froude number (Fr), general characteristics of the wind flow around the various islands can be inferred. The Froude number is defined as $\mathrm{Fr} = U/NH$, where U is the undisturbed up-

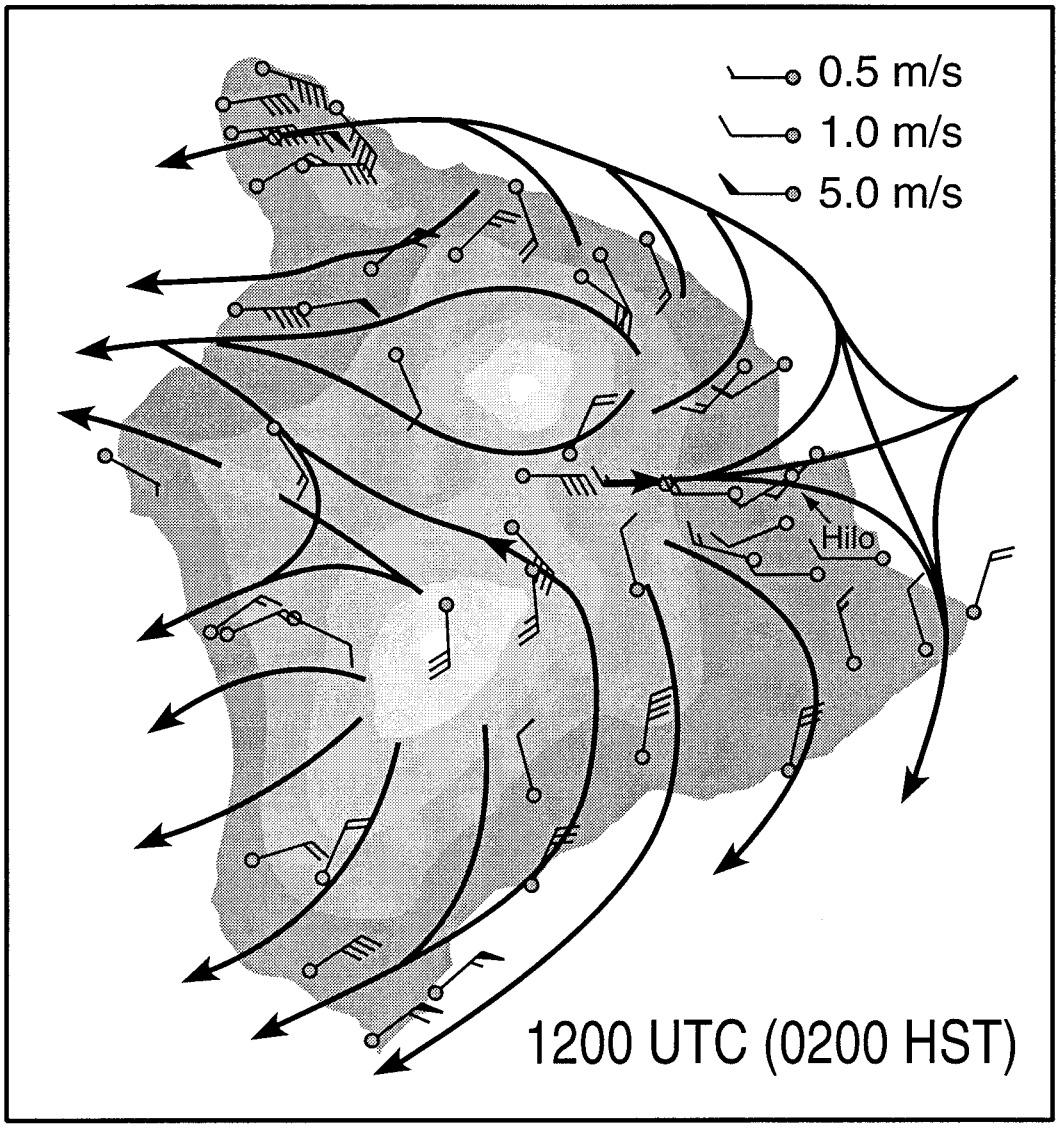

FIG. 12. Surface streamlines of average winds at 0200 local time during the Hawaiian Rainband Project (11 July–24 August 1990; adapted from Chen and Nash 1994). The plots are based on data from a network of 50 portable automated mesonet sites.

stream wind speed, N is the Brunt–Väisälä frequency, and H is the obstacle height. For islands with low Froude numbers such as the island of Hawaii (Fr $\sim$ 0.1 to 0.3), most of the airflows around the landmass. This has been confirmed by several observational (e.g., Leopold 1949; Chen and Nash 1994) and numerical modeling studies (e.g., Smolarkiewicz et al. 1988). Flow characteristics include a stagnation point just upstream of the island, and the deflection and acceleration of flow around the island (Fig. 12). The flow approaching those islands with higher average Froude numbers (e.g., Fr $>$ 1.0), such as the islands of Molokai and Guam, is generally able to move over the island.

The disruption of synoptic-scale flow by the complex island terrain produces localized high wind areas. These include gaps or passes in the mountains, along valleys, around the corners of the islands, and on lee slopes (Ramage et al. 1977). For example, the Ko'olau Range on Oahu induces damaging leeside winds several times each year. This mountain range is oriented northwest to southeast and presents a barrier normal to flow during strong northeasterly trade winds and southwesterlies ahead of advancing extratropical and subtropical cyclones. Schroeder (1977b) noted that this mountain range resembles the ''ramp-shaped'' barrier used by Klemp and Lilly (1975) to simulate wave-induced downslope winds, and mesoscale numerical models can simulate hydraulic jumps over Oahu (Lavoie 1974). Wave clouds in the lee of the island have been confirmed on satellite imagery (Burroughs and Larson 1979) and

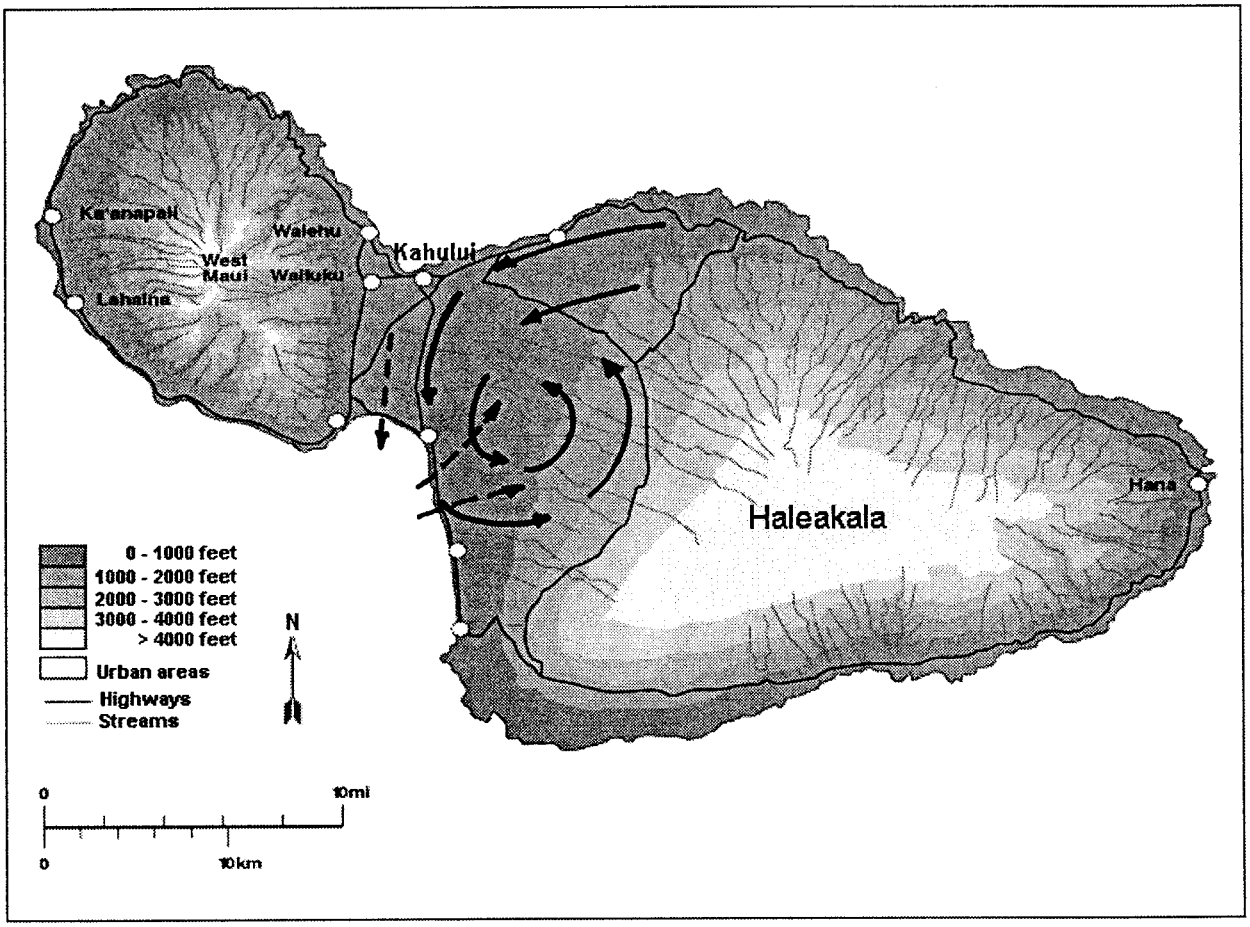

FIG. 13. Streamlines showing the ''Maui vortex.'' Based on composited data from 4 days of pilot balloon observations at 1200 local time. Dashed streamlines indicate winds at 305 m (1000 ft). Solid streamlines are for winds at 610–1219 m (2000–4000 ft; adapted from Leopold 1949).

have been used by glider pilots to set records for time aloft and altitude. Similar situations occur on the island of Tutuila in American Samoa. Tutuila is a narrow island with a northeast to southwest orientation and a 500-m mountain range along its major axis. This mountain range provides an obstacle perpendicular to the prevailing southeasterly trades as well as strong northwesterly winds that can develop during periods when the SPCZ axis is just to the southwest of the Samoa Islands. In the latter situations, gusty, damaging winds can occur in the lee of the mountain range.

Another example of a terrain-induced mesoscale feature is the Maui vortex. During trade wind conditions, the low-level trade flow is channeled through Maui's central valley between the West Maui Mountains and Haleakala volcano. The flow is then diverted eastward by a combination of the anabatic flow up Haleakala's west slope and deflection by the West Maui Mountains, resulting in a vortex that has been verified by wind data and cloud motion observations (Fig. 13). Pilot balloon observations show that this cyclonic eddy is best developed at ~1-km elevation with a return to trade wind flow above 2 km (Leopold 1949). Although cloud observations show the dissipation of the vortex cloud feature at night, computer simulations suggest that the vortex persists, though with a much weaker circulation (Ueyoshi et al. 1996). The ability of the Maui vortex to trap pollutants from agricultural burning makes this a feature of importance to forecasters (Schroeder 1993).

The smaller islands in the Pacific Region also produce terrain-induced features. For example, convergence of easterly winds in the lee of the island of Guam produces a frequently observed line of convection that can extend from the shoreline to as much as 200 km downstream. (M. Lander 1997, personal communication). Thunderstorms can form in this convergence zone with relatively frequent observations of lightning strikes on nearby coastal marine interests and waterspouts. Radar observations from the WSR-88D on Guam have shown the leeside convergence of easterlies in the radial wind velocity fields and rainfall estimates as high as 100 mm day^{-1}. Similar leeside convergence features are evident in satellite imagery over the Hawaiian Islands, though

thunderstorms are less frequent due to the stability of the prevailing trade wind regime.

c. Thermodynamic and diurnal effects

The role of thermodynamic circulations must also be taken into account during the forecast process. Land–sea and mountain–valley breezes are examples of thermodynamically induced circulations that are well developed, especially on the larger islands in the region. Using a transection of instrumented observation sites, Schroeder (1981) documented a sea breeze circulation that forms over the northwestern shore of the island of Hawaii. Because this region is largely sheltered from the trades by Mauna Kea (summit elevation 4.1 km), the sea breeze forms regularly. For the smaller islands such as Tutuila in American Samoa and Guam, a noticeable land–sea breeze circulation requires weak synoptic-scale flow. Several studies have documented good examples of mountain–valley breezes in the Hawaiian Islands, such as the circulation that develops over Haleakala volcano on the island of Maui (Lyons 1979) and over the Mauna Kea and Mauna Loa volcanoes on the island of Hawaii (e.g., Leopold 1949; Garrett 1980; Chen and Nash 1994). In fact, the combined nocturnal land breeze and katabatic wind that forms over the slopes of Mauna Loa is so persistent, the prevailing wind direction at the city of Hilo (on the eastern shore of the island) is from the west-southwest even though the northeasterly trade winds blow across the Hawaiian Islands 70% of the year (Fig. 12).

While the smaller islands and atolls in Micronesia experience weaker diurnal circulations, forecasters must account for the diurnal cycle of deep convective systems that frequently affect these locations. In a study using rain data from western North Pacific stations, Gray and Jacobson (1977) found a distinct diurnal signal in rain intensity. Maximum rainfall intensities tend to occur in the early morning hours close to local sunrise and minimum intensities in the late afternoon and early evening hours. The early morning maximum is hypothesized to be due to diurnal changes in tropospheric divergence resulting from a diurnal cycle of radiational cooling rates between the mesoscale disturbance areas and the clear areas surrounding the disturbance. Although Gray and Jacobson's results apply to deep convection, diurnal signals in trade wind convection have also been observed. For example, Brill and Albrecht (1982) show diurnal variations in the height of the trade wind inversion base, with a tendency for higher bases during the early morning hours and lower bases during the late afternoon. As a result, clouds tend to be deeper and precipitate more during the early morning hours. In addition to the diurnal cycle of trade wind convection, forecasters must also consider rainfall patterns related to diurnal island-scale circulations. Schroeder et al. (1977) document the diurnal cycle of rain on the main islands in the Hawaiian chain and show distinct diurnal patterns. The island of Hawaii provides an interesting example in which the diurnal cycle accounts for 64%–92% of the variance in the data. Over the east-facing slopes near sea level, rainfall frequency has a pronounced nocturnal maximum. The enhancement of offshore convergence by the combined land breeze/katabatic flow promotes the development of precipitating clouds that advect onshore. Windward upslope and leeward locations, however, experience rainfall frequency maxima in the afternoon hours as a result of cloud development from the combined sea breeze–anabatic flow.

d. Severe local storms

The Pacific Region also experiences its share of severe local storm events. Observations of funnel clouds are documented several times per year. Most of the funnels that reach the surface are in the form of waterspouts, though tornadoes are also observed (Fig. 14). Schroeder (1977a) found that most of the tornadoes that affect the Hawaiian Islands are weak and cause mostly minor damage. However, one case that occurred in Kailua-Kona (28 January 1971) on the island of Hawaii caused $1.5 million in damage. This was the most destructive tornado in Hawaii to date. Schroeder also noted that the ''typical'' Hawaiian funnel day is characterized by a significant synoptic-scale trough aloft to the west of the islands and the absence of trade winds and a trade wind inversion. As these synoptic-scale conditions occur mainly during the cool season, the maximum frequency of funnel observations (70%) occurs during this time.

On the island of Guam, waterspouts are common during the rainy season (June–October), and most are observed in association with a line of towering cumulus that extends offshore of the island during conditions of light easterly winds (Lander 1995). Lander also examined Doppler radar data from the WSR-88D on Guam and found the lack of a clear-cut vortex signature on a regular basis. This is consistent with findings by Wakimoto and Lew (1993) of Florida waterspouts during the Convection and Precipitation–Electrification experiment. In both studies, it is suggested that the WSR-88D is hard pressed to resolve the small horizontal scale of a typical waterspout vortex. An exception occurred near Guam on 3 September 1993, when radial velocity data showed tight anticyclonic rotation just to the southeast of the radar indicating the possibility of a waterspout. Visual confirmation of the waterspout was provided by observers. Another example is from the 25 January 1996 heavy rain event on Oahu. Radial velocity data from the Molokai WSR-88D (Fig. 15) show an inbound–outbound couplet approximately 40 km northeast of Oahu. The couplet also appears in scans from other elevation angles. An estimate of the mesocyclone's vertical component of vorticity is $\sim 10^{-2}$ s^{-1}, which is comparable to tornadic mesocyclones (Brandes 1993). In this case, due to the storm's distance from land, no waterspout confirmation is available.

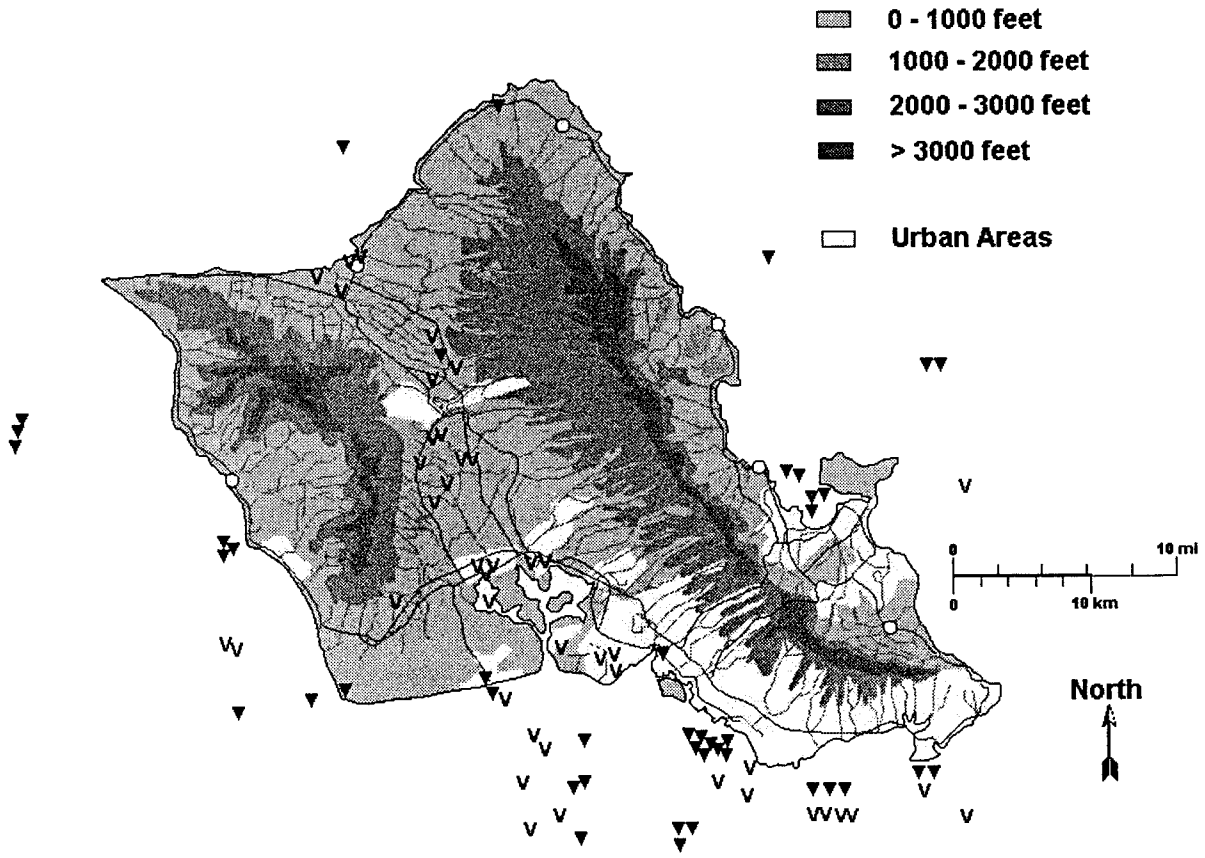

FIG. 14. Locations of reported funnels aloft (''v'' symbols) and waterspouts/tornadoes (triangles) for Oahu during the period 1961–75 (adapted from Schroeder 1977a).

In the Pacific Region most of the threat to life and property during thunderstorm activity (not associated with tropical cyclones) is due to heavy rains and attendant flash flooding. Destructive convective winds, lightning strikes, and hail storms are relatively rare, though there are spectacular exceptions. An example occurred on 22 May 1978 where a convective downburst estimated at 31 m s^{-1} over Kailua, Oahu, damaged boats and structures over a ~1.0 km × 2.0 km area (NCDC 1978). In a more recent example, convective gusts up to 41 m s^{-1} were reported with the passage of a strong squall line over the island of Kauai on 3 November 1995. The latter example is documented in detail in the accompanying article by Businger et al. (1998). The rarity of strong convective outflow events in the Pacific Region has been attributed to the presence of a deep moist layer that hinders the formation of evaporation-cooled downdrafts (e.g., Jorgensen et al. 1991; Kodama and Barnes 1997). Hail has occurred in scattered incidents across the tropical Pacific and most reports indicate sizes less than 6.4 mm (0.25 in.) in diameter (Frisby and Sansom 1967; Blumenstock and Price 1967). Low vertical velocities of convective-scale updrafts in oceanic convection (Jorgensen and LeMone 1989) as well as the warm temperatures of the lower tropical troposphere are likely factors contributing to the rarity of hail.

5. Modernization and collaboration

Over the past several years, the NWS has been involved in a major modernization and associated restructuring program that is designed to upgrade and carry its operational forecasting capabilities into the twenty-first century. Across the United States outdated equipment is being replaced with new systems such as the WSR-88D radar, the Automated Surface Observing System (ASOS), the next-generation Geostationary Operational Environmental Satellite (GOES), and the Advanced Weather Interactive Processing System (AWIPS). Various aspects of the NWS MAR as it pertains to the Pacific region and other local modernization efforts will be briefly discussed here.

a. The WSR-88D system

Of all the various improvements resulting from the MAR to date, the installation of the WSR-88D radar system at several sites in the Hawaiian Islands and on Guam has, arguably, had the greatest impact on local forecast

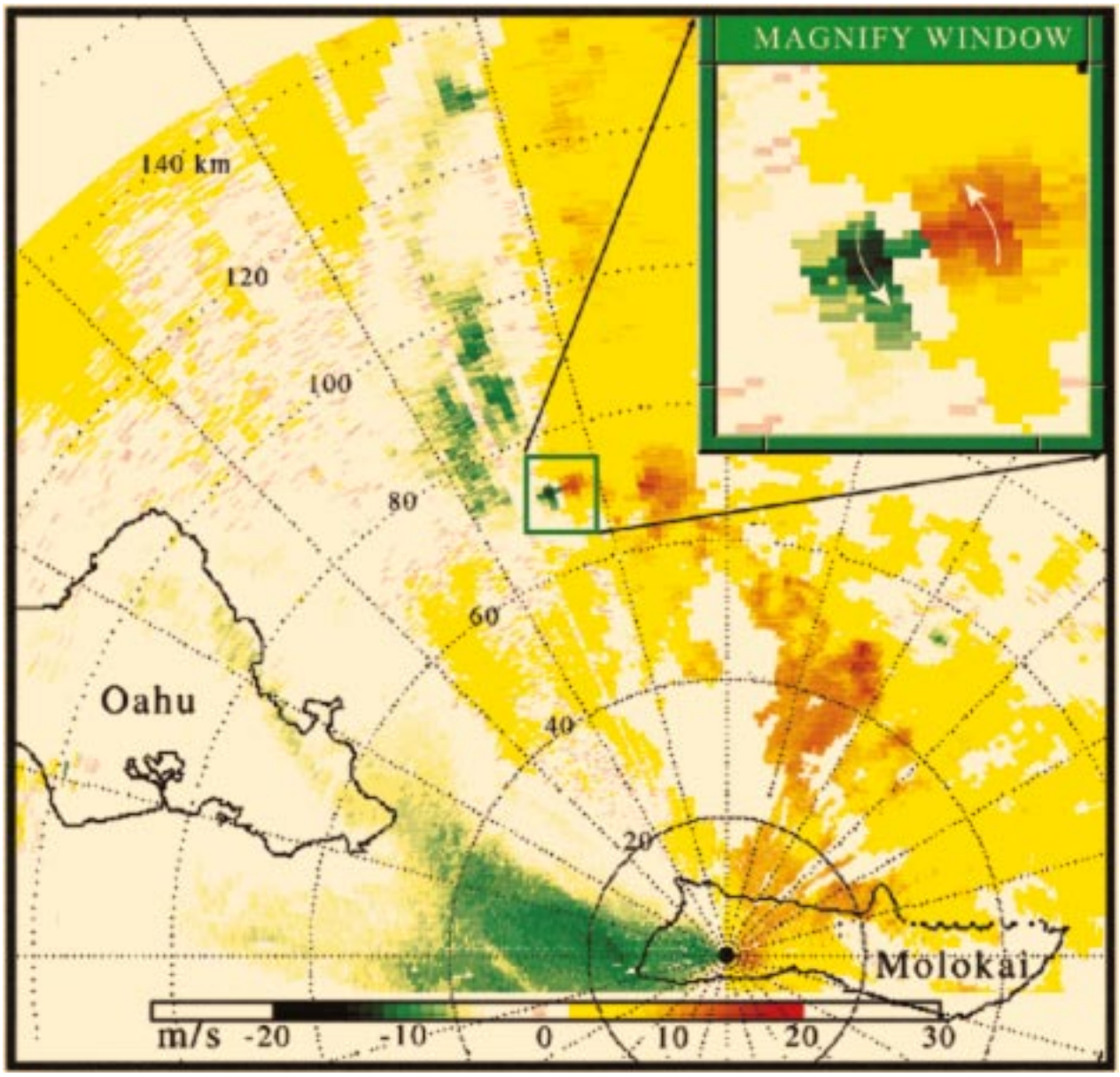

FIG. 15. Mesocyclone signature in radial velocity data (m s^{-1}) from the Molokai WSR-88D radar on 0334 UTC 25 January 1996. Range rings in km.

office operations. Four WSR-88D sites have been installed across the Hawaiian Islands, providing nearly complete spatial coverage (at 3048 m, or 10 000 ft) over the island chain (Fig. 16). The first two WSR-88D radars, installed on the islands of Kauai and Molokai, have already proven to be beneficial to the public by improving severe weather and heavy rain detection and flash flood warning capability. An example is the Kauai severe weather event from 3 November 1995. Using reflectivity and radial velocity data from the Kauai WSR-88D, forecasters issued a severe thunderstorm warning, rare for the Hawaiian Islands, that verified with significant lead time. This event is described in greater detail in an accompanying article by Businger et al. (1998).

In addition to its severe weather capabilities, the WSR-88D system also contains important hydrometeorological functions as part of its precipitation processing system (PPS). Radar reflectivity data can be converted to a rain rate and integrated to provide high temporal and spatial resolution rainfall data. However, it has been found that the default reflectivity-to-rainfall (Z–R) relationship currently used by the PPS results in significant underestimates of rainfall in tropical regimes (e.g., Choy et al. 1996; Garza 1995; Lander 1995). In

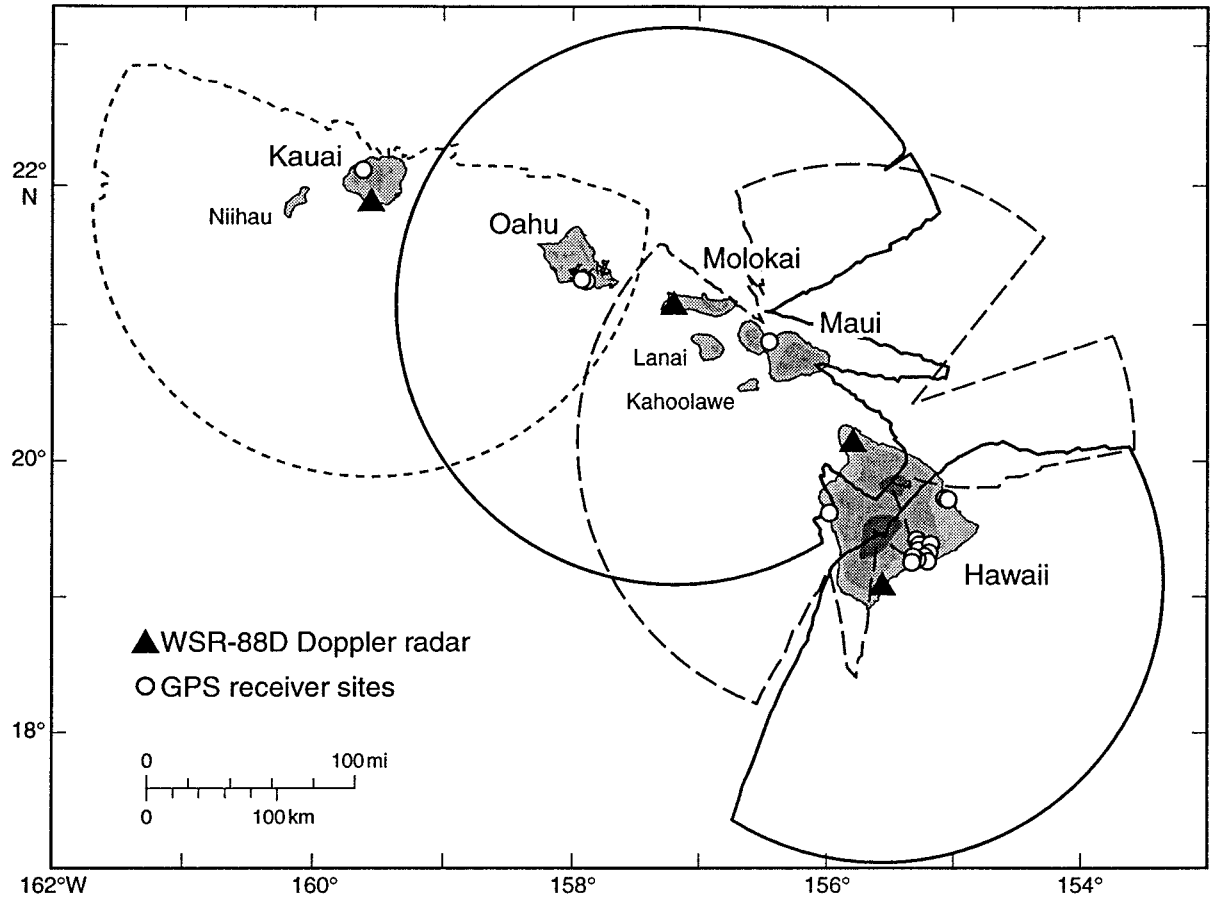

FIG. 16. WSR-88D coverage at 3048 m (10 000 ft) above site level over the Hawaiian Islands. Due to the complex island terrain, blind spots remain after full deployment of all the radars. Triangles indicate locations of the four WSR-88D radars. Small open circles indicate locations of geodetic GPS receivers.

a collaborative project between the University of Hawaii's Department of Meteorology and the WSFO Honolulu, research is being conducted to try and reduce algorithmic biases in the PPS. Initial findings for the island of Oahu show that use of a modified *Z–R* relationship still results in underestimates of the observed rainfall, though much improved over the default relationship (T. Birchard and P. Jendrowski 1997, personal communication).

The WSR-88D system on Guam is providing unprecedented details to operational forecasters on tropical cyclones that approach the Northern Mariana Islands. Forecasters find the high temporal resolution of the wind data particularly useful in gauging the strength of the winds that can occur with a tropical cyclone. In a case study on the passage of Tropical Cyclone Ed over Guam in 1993, Stewart and Lyons (1996) note that land-based surface wind observations correlate extremely well with 75%–80% of the 1500-m radial velocity estimates.

b. ASOS

ASOS will be installed at nine sites across the Pacific region in support of aviation operations. The benefits of ASOS include an increase in the temporal resolution of surface observations as well as a continuous weather watch capability where only part-time or no observations are currently taken (Friday 1994). However, ASOS cannot replace a trained human observer's ability to report critical phenomena such as tornadoes/funnel clouds and thunderstorms in the vicinity of the observation site. This limitation will be overcome at select locations by supplemental observations taken by certified observers as required.

c. GOES and other remote sensing platforms

Due to the paucity of observations across the Pacific Ocean, weather forecasters in the Pacific region depend heavily on satellite imagery for their operations. This includes data from the GOES, the Japanese Geostationary Meteorological Satellite (GMS), and the National Oceanic and Atmospheric Administration series of polar orbiting satellites. In the past, processed GOES imagery was available every 30 min for the infrared, visible, and water vapor wavelength channels. Full-disk imagery from the GMS satellite was available every 3 h via

facsimile circuit for both the infrared and visible channels. Water vapor imagery was not available. Data from both satellites allowed Pacific region forecasters to view the entire Pacific. However, during periods when only one GOES satellite was operational, data over the central Pacific suffered from considerable parallax-induced cloud displacements as the region was on the edge of the GOES and GMS satellites' field of view.

The launch of the new GOES and GMS satellites as well as the improvements in data processing and display technology gives forecasters the ability to monitor changing weather conditions more effectively. Geostationary satellite coverage over the eastern Pacific Ocean is now provided by the *GOES-9* (over 135°W) satellite, while the western Pacific is covered by the *GMS-5* (over 140°E) satellite. Updated digital images from *GOES-9*, with a 1-km resolution in the visible wavelengths and 4 km in the infrared, are now available routinely every 15 min (soon to be every 7.5 min). Direct access to 1.25-km resolution visible and 5-km infrared digital *GMS-5* imagery is now available routinely every hour. Furthermore, communication and computer upgrades now allow Pacific region forecasters to overlay observations from other data sources (e.g., buoys and surface stations). Planned software upgrades will focus on the utilization of additional imager wavelengths and separate sounder data from *GOES-9*. For example, algorithms are being developed to derive precipitable water from the *GOES-9* 11 and 12-μm channels. These data can be used to gauge moisture flux convergence in the vicinity of thunderstorms and have the potential to provide an important constraint for regional numerical weather prediction models.

In addition to the conventional visible, infrared, and water vapor channel images, newer hybrid products have proven to be quite useful to forecasters. A good example is wind data derived from the water vapor channel of geostationary satellites (Velden 1996). Like the long-used cloud motion winds product, the water vapor winds product identifies and tracks features in the imagery to determine the wind field in the upper troposphere. The advantage of the water vapor winds technique is that the wind vector fields can be derived for both cloudy and cloud-free regions and the height of the winds can be well estimated (Nieman et al. 1993). Tropical cyclone forecasters at the JTWC on Guam have found these data to be a useful supplement to improve the upper-tropospheric wind analyses for the western Pacific Ocean.

More recently, data from the Defense Meteorological Satellite Program (DMSP) satellites and the European Remote Sensing 2 (*ERS-2*) satellite have been made available for use in operational forecasts. The active *ERS-2* and passive DMSP microwave sensors each provide high-resolution surface wind data that help fill-in the data-sparse areas of the Pacific. Both the JTWC on Guam and the CPHC in Honolulu have found these data to be useful in determining tropical cyclone location and intensity.

Another new remote sensing technology is the use of the Global Positioning Satellites (GPS) for atmospheric monitoring. L-band radio signals transmitted by GPS satellites are delayed (refracted) by atmospheric water vapor as they propagate to ground-based GPS receivers. This ''wet delay'' is nearly proportional to the quantity of water vapor integrated along the signal path. The ability of GPS to accurately measure integrated water vapor and the utility of the resulting data in meteorological analysis have been demonstrated through the GPS/STORM experiment and the subsequent data analysis (Businger et al. 1996). A network of continuously operating GPS receivers, including approximately 25 receivers outfitted with surface barometers, is currently being constructed across the state of Hawaii for a combination of geodetic, meteorological, and navigation purposes (Fig. 16). A number of receivers are already in place, including U.S. Coast Guard and U.S. Geodetic Survey receivers. The installation phase of the network is scheduled to be essentially complete in the summer of 1998. The integrated water vapor data will be used to enhance the initial state of the island-scale nest in the Regional Spectral Model (see section 5g), and the output of the model will be used in turn to evaluate the contribution of the GPS data to the accuracy of the simulation.

d. AWIPS

The AWIPS will be deployed in the Pacific region in the near future and is expected to greatly enhance NWS forecast office operational capabilities. AWIPS will be responsible for receiving and processing hydrometeorological data from a wide variety of sources including ASOS, WSR-88D, and GOES. In its final form, forecasters will use AWIPS for data analysis and the generation of a database from which all graphical and draft text forecast products will be created.

e. The Hawaii Rainfall Monitoring System

Due to the rapid response times of Hawaiian streams, effective flash flood warnings require the timely detection of the onset of heavy rain. In the past, the detection capability in the Hawaiian Islands was severely limited. Conventional radar data were not available on a routine basis and telemetered rain gauges were few in number and did not automatically notify the forecasters of heavy rain onset (e.g., Schroeder 1977c). Thus, information on the occurrence of heavy rains often came from eyewitness reports from law enforcement officials, civil defense, or the general public.

Since 1994, a modernized network of telemetered rain gauges has been providing real-time rainfall data to the WSFO Honolulu in support of its hydrology program. The installation of the network, known as the Hawaiian

Rainfall Monitoring System (HRMS), is in response to recent severe flooding events across the island chain. Some notable examples are the Oahu New Year's Eve flood [31 December 1987–1 January 1988; approximately $35 million in damage; Department of Land and Natural Resources (1988)] and the Anahola flood on Kauai [13–14 December 1991; four fatalities; Department of Land and Natural Resources (1992)]. At the present time, the HRMS rain gauge network consists of 70 Limited Automatic Remote Collection (LARC) tipping-bucket gauges that are automatically interrogated every 6 h by a forecast office computer. Each LARC is also programmed to alarm forecasters if rainfall intensities exceed user-defined thresholds. It is important to note that the HRMS is an important complement to the WSR-88Ds and has not been replaced by the Doppler radar in Hawaii's flash flood program. Real-time, telemetered gauge data, as in other locations around the United States, provide important ground-truth and calibration information to the WSR-88D's precipitation processing system, and as previously mentioned, progress is being made toward accounting for biases in the radar's precipitation estimates.

f. Collaboration efforts

The Pacific Region is actively involved in collaboration between the NWS and the university research community. The guiding principles of this collaboration are to (i) optimize the utility of the new observing systems as data resources for forecasting; (ii) conduct case studies and climatological analyses of significant weather events to develop better conceptual models of the weather systems that produce these events; (iii) develop a high-resolution mesoscale numerical model capability, with regional data enhancement; (iv) use NWS national centers and GPS data streams to develop diagnostic forecasting tools and algorithms that focus on the mesoscale–nowcasting aspect of weather forecasting; and (v) promote the exchange of information and understanding concerning weather forecasting in the Tropics.

In June 1995, the new WSFO Honolulu office opened on the campus of the University of Hawaii—Manoa (UH). The collocation of this office with the UH Department of Meteorology fosters an excellent environment for interaction and research collaboration between operational forecasters and university researchers and students. All of the Pacific region articles in this special issue are a direct result of the collocation and increased collaboration. In addition to research, collaborative training is an important part of the Pacific region's activities. Examples include the 1995 Cooperative Program for Operational Meteorology, Education and Training Tropical Mesoscale Meteorology Workshop and the ongoing series of operationally oriented satellite meteorology courses being taught by the University of Guam.

g. Operational mesoscale modeling

Recent advances at NCEP have brought operational mesoscale model guidance to the WSFO Honolulu. This guidance comes from the hydrostatic version of the RSM, a proven model with statistical verification scores comparable to other operational NCEP regional models (e.g., Eta) and a large array of postprocessed diagnostic fields available for forecaster use (Juang and Kanamitsu 1994; Juang et al. 1997). The Hawaiian domain RSM uses initial conditions from the NCEP T126 Global Spectral Model (GSM) and two nested grids to produce output at approximately 10-km horizontal resolution. It employs an identical structure and physics package as the GSM, which is the principal operational model for the Pacific Region. Commonality with the GSM reduces errors and results in more efficient processing on an already tight NCEP computer schedule. In addition, the global domain of the GSM permits easy future movement of the RSM to other Pacific Region domains (e.g., Guam or American Samoa) as computational resources become available.

Early RSM verification results over Hawaii show that although the 10-km hydrostatic version provides added value to the GSM forecast, the resolution is still insufficient to accurately depict some of the significant mesoscale features that develop over very small spatial scales in the complex island terrain. A nonhydrostatic version of the RSM at ~1–3 km resolution is under development for the Hawaiian domain and will hopefully improve upon the guidance provided by the 10-km hydrostatic version.

The RSM has also been installed on a local workstation at the UH Department of Meteorology as part of an NWS–UH collaborative project. The locally run RSM is identical to the operational 10-km version and is used for model improvement, data enhancement for initial conditions, and case studies. An accompanying article by Wang et al. (1998) discusses in greater detail the application of the RSM for forecasting in the Hawaiian Islands.

6. Summary and closing remarks

Forecasters in the Pacific Region of the National Weather Service face the unique and challenging responsibility of providing forecasts and issuing weather advisories, watches, and warnings over a domain more than twice the size of the continental United States. Within this forecast domain, extratropical, subtropical, and tropical systems with a wide range of temporal and spatial scales must be considered on a daily basis. In addition, forecasters must account for orographic and diurnal influences that significantly affect local weather conditions.

Compounding the forecast challenge is a lack of in situ data over the Pacific Ocean. New observational tools such as the WSR-88D radar system and the GOES

I–M series of satellites have helped mitigate this problem and have already resulted in more effective forecasts and warnings for the public. Furthermore, collaborative research and training activities have increased considerably during recent years, especially since the collocation of the WSFO Honolulu on the University of Hawaii campus. This paper and the accompanying Pacific Region articles are products of this increased collaboration. The value of these efforts has been appreciated at all levels and it is anticipated that future collaborative efforts will continue to pay dividends.

Acknowledgments. The authors wish to thank Tom Schroeder, Gary Barnes, Mark Lander, Paul Jendrowski, Hann-Ming ''Henry'' Juang, and James Partain for their insightful comments and suggestions. Comments by the two reviewers also helped improve the presentation of the paper. Brooks Bays provided graphical assistance on several of the figures. This paper is funded, in part, by Cooperative Agreement NA37RJ0199 from the National Oceanic and Atmospheric Administration and through the UCAR COMET Outreach Program under Grant UCAR S94-43844. The views expressed herein are those of the authors and do not necessarily reflect the views of NOAA or any of its subagencies.

REFERENCES

Barnes, G. B., and K. Sieckman, 1984: The environment of fast- and slow-moving tropical mesoscale convective cloud lines. *Mon. Wea. Rev.,* **112,** 1782–1794.

Bjerknes, J., 1969: Atmospheric teleconnections from the equatorial Pacific. *Mon. Wea. Rev.,* **97,** 163–172.

Blumenstock, D. L., and S. Price, 1967: Climates of the United States—Hawaii. Climatography of the United States 60-51, U.S. Dept. of Commerce, ESSA, 27 pp. [Available from NOAA Central Library, 2d Floor, SSMC3, 1315 East–West Highway Silver Spring, MD 20910.]

Brandes, E. A., 1993: Tornadic thunderstorm characteristics determined with Doppler radar. *The Tornado: Its Structure, Dynamics, Prediction, and Hazards, Geophys. Monogr.,* No. 79, Amer. Geophys. Union, 143–159.

Brill, K., and B. Albrecht, 1982: Diurnal variation of the trade-wind boundary layer. *Mon. Wea. Rev.,* **110,** 601–613.

Burroughs, L. D., and R. N. Larson, 1979: Wave clouds in the vicinity of Oahu Island, Hawaii. *Mon. Wea. Rev.,* **107,** 608–611.

Businger, S., and Coauthors, 1996: The promise of GPS in atmospheric monitoring. *Bull. Amer. Meteor. Soc.,* **77,** 5–18.

——, T. Birchard, K. Kodama, P. A. Jendrowski, and J. J. Wang, 1998: A bow echo and severe weather associated with a kona low in Hawaii. *Wea. Forecasting,* **13,** 306–321.

Chen, Y. L., and A. J. Nash, 1994: Diurnal variation of surface airflow and rainfall frequencies on the island of Hawaii. *Mon. Wea. Rev.,* **122,** 34–56.

Choy, B. K., L. Mazarowski, and P. Glitto, 1996: Tropical Storm Gordon: 72-hr rainfall totals over east central Florida and WSR-88D comparisons. NOAA Tech. Memo. NWS SR-174, 18 pp. [Available from NOAA/SRH-SSD, 819 Taylor St., Room 10A26, Fort Worth, TX 76102.]

Chu, P. S., 1995: Hawaii rainfall anomalies and El Niño. *J. Climate,* **8,** 1697–1703.

——, and J. Frederick, 1990: Westerly wind bursts and surface heat fluxes in the equatorial western Pacific in May 1982. *J. Meteor. Soc. Japan,* **68,** 523–537.

Chun, A. K. T., R. T. Martin, H. E. Rosendal, and G. H. Trapp, 1993: 1992 tropical cyclones—Central North Pacific. NOAA Tech. Memo. NWSTM PR-38, 71 pp. [Available from NOAA/PRH, Grosvenor Center—Mauka Tower, 737 Bishop St., Ste. 2200, Honolulu, HI 96813.]

Cotton, W. R., and R. A. Anthes, 1989: *Storm and Cloud Dynamics.* Academic Press, 883 pp.

Cram, R. S., and H. R. Tatum, 1979: Record torrential rainstorms on the island of Hawaii, January–February 1979. *Mon. Wea. Rev.,* **107,** 1653–1662.

Department of Land and Natural Resources, 1988: Post flood report: New Year's Eve storm, December 31, 1987–January 1, 1988, windward and leeward east Oahu. Circular 119, Honolulu, HI, 55 pp. [Available from Department of Land and Natural Resources, Division of Water and Land Development, State of Hawaii, P.O. Box 373, Honolulu, HI 96809.]

——, 1992: Post flood report: Storm of December 14, 1991, northeast Kauai. Circular C121, Honolulu, HI, 35 pp. [Available from Department of Land and Natural Resources, Division of Water and Land Development, State of Hawaii, P.O. Box 373, Honolulu, HI 96809.]

Dorman, C. E., and R. H. Bourke, 1979: Precipitation over the Pacific Ocean, 30°S to 60°N. *Mon. Wea. Rev.,* **107,** 896–910.

Elliot, W. P., and R. K. Reed, 1984: A climatological estimate of precipitation for the world ocean. *J. Climate Appl. Meteor.,* **23,** 434–439.

Friday, E. W., 1994: The modernization and associated restructuring of the National Weather Service: An overview. *Bull. Amer. Meteor. Soc.,* **75,** 43–52.

Frisby, E. M., and H. W. Sansom, 1967: Hail incidence in the Tropics. *J. Appl. Meteor.,* **6,** 339–354.

Gamache, J. F., and R. A. Houze, 1983: Water budget of a mesoscale convective system in the Tropics. *J. Atmos. Sci.,* **40,** 1835–1850.

Garrett, A. J., 1980: Orographic cloud over the eastern slopes of Mauna Loa volcano, Hawaii, related to insolation and wind. *Mon. Wea. Rev.,* **108,** 931–941.

Garza, A. L., 1995: A comparison of two winter-type heavy rainfall events in Hawaii—Kona storm and upper-tropospheric trough flash flood producers. NOAA Tech. Memo. NWSTM PR-40, 33 pp. [Available from NOAA/PRH, Grosvenor Center-Mauka Tower, 737 Bishop St., Ste. 2200, Honolulu, HI 96813.]

——, G. H. Trapp, B. Hablutzel, H. E. Rosendal, R. Farrell, R. Matsuda, and J. Hoag, 1995: 1994 tropical cyclones—Central North Pacific. NOAA Tech. Memo. NWSTM PR-41, 103 pp. [Available from NOAA/PRH, Grosvenor Center-Mauka Tower, 737 Bishop St., Ste. 2200, Honolulu, HI 96813.]

Giambelluca, T. W., L. S. Lau, Y. S. Fok, and T. A. Schroeder, 1986: Rainfall atlas of Hawaii. Rep. R-76, Water Resources Research Center, University of Hawaii, Honolulu, HI, 267 pp. [Available from Department of Land and Natural Resources, Division of Water and Land Development, State of Hawaii, P.O. Box 373, Honolulu, HI 96809.]

Gray, W. M., 1985: Tropical cyclone global climatology. Tech. Document WMO/TD 72, Vol. I, WMO, Geneva, Switzerland, 319 pp. [Available from World Meteorological Organization, P.O. Box 2300, CH-1211 Geneva 2, Switzerland.]

——, and R. W. Jacobson, 1977: Diurnal variation of deep cumulus convection. *Mon. Wea. Rev.,* **105,** 1171–1188.

Grindinger, C. M., 1992: Temporal variability of the trade wind inversion: Measured with a boundary layer vertical profiler. M.S. thesis, Dept. of Meteorology, University of Hawaii, 93 pp. [Available from Dept. of Meteorology, University of Hawaii, 2525 Correa Rd., Honolulu, HI 96822.]

Guard, C. P., L. E. Carr, F. H. Wells, R. A. Jeffries, N. D. Gural, and D. K. Edson, 1992: Joint Typhoon Warning Center and the challenges of multibasin tropical cyclone forecasting. *Wea. Forecasting,* **7,** 328–352.

Harr, P. A., R. L. Elsberry, and J. C. L. Chan, 1996: Transformation of a large monsoon depression to a tropical storm during TCM-93. *Mon. Wea. Rev.,* **124,** 2625–2643.

Holland, G. J., 1984: On the climatology and structure of tropical cyclones in the Australian/southwest Pacific region: II. Hurricanes. *Aust. Meteor. Mag.*, **32,** 17–31.

Horel, J. D., and J. M. Wallace, 1981: Planetary-scale atmospheric phenomena associated with the Southern Oscillation. *Mon. Wea. Rev.*, **109,** 813–829.

Houze, R. A., 1977: Structure and dynamics of a tropical squall-line system. *Mon. Wea. Rev.*, **105,** 1540–1567.

——, and A. K. Betts, 1981: Convection in GATE. *Rev. Geophys. Space Phys.*, **19,** 541–576.

Jorgensen, D. P., and M. A. LeMone, 1989: Vertical velocity characteristics of oceanic convection. *J. Atmos. Sci.*, **46,** 621–640.

——, ——, and B. Jou, 1991: Precipitation and kinematic structure of an oceanic mesoscale convective system. Part I: Convective line structure. *Mon. Wea. Rev.*, **119,** 2608–2637.

——, ——, and S. B. Trier, 1997: Structure and evolution of the 22 February 1993 TOGA COARE squall line: Aircraft observations of precipitation, circulation, and surface energy fluxes. *J. Atmos. Sci.*, **54,** 1961–1985.

Juang, H.-M. H., and M. Kanamitsu, 1994: The NMC nested regional spectral model. *Mon. Wea. Rev.*, **122,** 3–26.

——, S.-Y. Hong, and M. Kanamitsu, 1997: The NCEP regional spectral model: An update. *Bull. Amer. Meteor. Soc.*, **78,** 2125–2143.

JTWC, 1993: 1993 annual tropical cyclone report. Joint Typhoon Warning Center, 243 pp. [Available from JTWC PSC 489, Box 12, FPO AP 96536-0051.]

Keen, R. A., 1982: The role of cross-equatorial tropical cyclone pairs in the Southern Oscillation. *Mon. Wea. Rev.*, **110,** 1405–1416.

Kelley, W. E., and D. R. Mock, 1982: A diagnostic study of upper tropospheric cold lows over the western North Pacific. *Mon. Wea. Rev.*, **110,** 471–480.

Klemp, J. B., and D. K. Lilly, 1975: The dynamics of wave-induced downslope winds. *J. Atmos. Sci.*, **32,** 320–339.

Kloesel, K. A., and B. A. Albrecht, 1989: Low-level inversions over the tropical Pacific—Thermodynamic structure of the boundary layer and the above-inversion moisture structure. *Mon. Wea. Rev.*, **117,** 87–101.

Kodama, K., and G. M. Barnes, 1997: Heavy rain events over the south-facing slopes of Hawaii: Attendant conditions. *Wea. Forecasting*, **12,** 347–367.

Lander, M. A., 1990: Evolution of the cloud pattern during the formation of tropical cyclone twins symmetrical with respect to the equator. *Mon. Wea. Rev.*, **118,** 1194–1202.

——, 1994: An exploratory analysis of the relationship between tropical storm formation in the western North Pacific and ENSO. *Mon. Wea. Rev.*, **122,** 636–651.

——, 1995: Exploring the atmosphere of the deep tropics with Guam's NEXRAD. Preprints, *Tropical Mesoscale Meteorology Symp.*, Honolulu, HI, Cooperative Program for Operational Meteorology, Education and Training. [Available from NOAA/PRH, Grosvenor Center-Mauka Tower, 737 Bishop St., Ste. 2200, Honolulu, HI 96813.]

——, 1996: Specific tropical cyclone track types and unusual tropical cyclone motions associated with a reverse-oriented monsoon trough in the western North Pacific. *Wea. Forecasting*, **11,** 170–186.

Larson, R. N., 1976: Cumulus line formation in the trade wind easterlies. Satellite Applications Information Note 76/20, NWS/NESS, 5 pp. [Available from NOAA/NESDIS Satellite Applications Laboratory, Washington, DC 20233.]

Lavoie, R. L., 1974: A numerical model of trade wind weather on Oahu. *Mon. Wea. Rev.*, **102,** 630–637.

Leary, C. A., and R. A. Houze, 1979: The structure and evolution of convection in a tropical cloud cluster. *J. Atmos. Sci.*, **36,** 437–457.

LeMone, M. A., and E. J. Zipser, 1980: Cumulonimbus vertical velocity events in GATE. Part I: Diameter, intensity and mass flux. *J. Atmos. Sci.*, **37,** 2444–2457.

Leopold, L. B., 1949: The interaction of trade wind and sea breeze, Hawaii. *J. Meteor.*, **6,** 312–320.

Levinson, D., 1990: Synoptic and subsynoptic aspects of a Hawaiian frontal zone. M.S. thesis, Dept. of Meteorology, University of Hawaii, 65 pp. [Available from Dept. of Meteorology, University of Hawaii, 2525 Correa Rd., Honolulu, HI 96822.]

Lukas, R., S. P. Hayes, and K. Wyrtki, 1984: Equatorial sea level response during the 1982–1983 El Niño. *J. Geophys. Res.*, **89** (C6), 10 425–10 430.

Luther, D. S., D. E. Harrison, and R. A. Knox, 1983: Zonal winds in the central equatorial Pacific and El Niño. *Science*, **222,** 327–330.

Lyons, S. W., 1979: Summer weather on Haleakala, Maui. UH-MET 79-09, Dept. of Meteorology, University of Hawaii, 56 pp. [Available from Dept. of Meteorology, University of Hawaii, 2525 Correa Rd., Honolulu, HI 96822.]

Madden, R. A., and P. R. Julian, 1971: Detection of a 40–50 day oscillation in the zonal wind in the tropical Pacific. *J. Atmos. Sci.*, **28,** 702–708.

——, and ——, 1994: Observations of the 40–50-day tropical oscillation—A review. *Mon. Wea. Rev.*, **122,** 814–837.

Maddox, R. A., 1980: Mesoscale convective complexes. *Bull. Amer. Meteor. Soc.*, **61,** 1374–1387.

Miller, D., and J. M. Fritsch, 1991: Mesoscale convective complexes in the western Pacific region. *Mon. Wea. Rev.*, **119,** 2978–2992.

Murakami, T., and W. L. Sumathipala, 1989: Westerly wind bursts during 1982/83 ENSO. *J. Climate*, **2,** 71–85.

Nakazawa, T., 1988: Tropical super clusters within intraseasonal variations over the western Pacific. *J. Meteor. Soc. Japan*, **66,** 823–839.

NCDC, 1978: *Storm Data.* Vol. 20, No. 5, 24 pp.

——, 1996: *International Station Meteorological Climate Summary.* Version 4.0, National Climatic Data Center, CD-ROM. [Available from the National Climatic Data Center, Federal Building, 151 Patton Ave., Asheville, NC 28801.]

Nieman, S. J., J. Schmetz, and W. P. Menzel, 1993: A comparison of several techniques to assign heights to cloud tracers. *J. Appl. Meteor.*, **32,** 1559–1568.

Philander, S. G. H., 1985: El Niño and La Niña. *J. Atmos. Sci.*, **42,** 2652–2662.

Ramage, C. S., 1962: The subtropical cyclone. *J. Geophys. Res.*, **67,** 1401–1411.

——, 1971: *Monsoon Meteorology.* Academic Press, 296 pp.

——, 1986: El Niño. *Sci. Amer.*, **254,** 76–83.

——, 1995: Forecasters guide to tropical meteorology, AWS TR 240 Updated. AWS/TR-95/001, Air Weather Service, U.S. Air Force, 392 pp. [Available from AWSTL, 859 Buchanan St., Scott AFB, IL 62225.]

——, P. A. Daniels, T. A. Schroeder, and N. J. Thompson, 1977: Oahu wind survey, first report. UHMET 77-01, Dept. of Meteorology, University of Hawaii, 42 pp. [Available from Dept. of Meteorology, University of Hawaii, 2525 Correa Rd., Honolulu, HI 96822.]

——, S. J. S. Khalsa, and B. N. Meisner, 1981: The central Pacific near-equatorial convergence zone. *J. Geophys. Res.*, **86,** 6580–6598.

Rasmussen, E. M., and T. H. Carpenter, 1982: Variations in tropical sea surface temperature and surface wind fields associated with the Southern Oscillation/El Niño. *Mon. Wea. Rev.*, **110,** 354–384.

Raymond, D. J., and S. A. Lewis, 1995: Rotating convective disturbances in the trades. *Quart. J. Roy. Meteor. Soc.*, **121,** 271–299.

Riehl, H., 1954: *Tropical Meteorology.* McGraw-Hill, 392 pp.

Ropelewski, C. F., and M. S. Halpert, 1987: Global and regional scale precipitation patterns associated with the El Niño/Southern Oscillation. *Mon. Wea. Rev.*, **115,** 1606–1626.

——, and ——, 1989: Precipitation patterns associated with the high index phase of the Southern Oscillation. *J. Climate*, **2,** 268–284.

Sadler, J. C., 1967: The tropical upper tropospheric trough as a sec-

ondary source of typhoons and a primary source of tradewind disturbances. Hawaii Institute of Geophysics Rep. HIG-67-12, 44 pp. [Available from Dept. of Meteorology, University of Hawaii, 2525 Correa Rd., Honolulu, HI 96822.]

——, 1976: A role of the tropical upper tropospheric trough in early season typhoon development. *Mon. Wea. Rev.*, **104,** 1266–1278.

——, 1984: The anomalous tropical cyclones in the Pacific during the 1982–83 El Niño. Preprints, *15th Conf. on Hurricanes and Tropical Meteorology*, Miami, FL, Amer. Meteor. Soc., 51–55.

——, M. A. Lander, A. M. Hori, and L. K. Oda, 1987: Tropical marine climatic atlas, Volume II, Pacific Ocean. UH-MET 87-02, Dept. of Meteorology, University of Hawaii, 27 pp. [Available from Dept. of Meteorology, University of Hawaii, 2525 Correa Rd., Honolulu, HI 96822.]

Schroeder, T. A., 1977a: Hawaiian waterspouts and tornadoes. *Mon. Wea. Rev.*, **105,** 1163–1170.

——, 1977b: Severe downslope winds on Oahu. Preprints, *10th Conf. on Severe Local Storms*, Omaha, NE, Amer. Meteor. Soc., 373–375.

——, 1977c: Meteorological analysis of an Oahu flood. *Mon. Wea. Rev.*, **105,** 458–468.

——, 1981: Characteristics of local winds in northwest Hawaii. *J. Appl. Meteor.*, **20,** 874–881.

——, 1993: Climate controls. *Prevailing Trade Winds*, M. Sanderson, Ed., University of Hawaii Press, 12–36.

——, and Z. P. Yu, 1995: Interannual variability of central Pacific tropical cyclones. Preprints, *21st Conf. on Hurricanes and Tropical Meteorology*, Miami, FL, Amer. Meteor. Soc., 437–438.

——, B. J. Kilonsky, and B. N. Meisner, 1977: Diurnal variation in rainfall and cloudiness. UH-MET 77-03, Dept. of Meteorology, University of Hawaii, 67 pp. [Available from Dept. of Meteorology, University of Hawaii, 2525 Correa Rd., Honolulu, HI 96822.]

Shaw, S. L., 1981: A history of tropical cyclones in the central North Pacific and the Hawaiian Islands: 1832–1979. NOAA, 137 pp. [Available from NOAA Central Library, 2d Floor, SSMC3, 1315 East–West Highway, Silver Spring, MD 20910.]

Simpson, R. H., 1952: Evolution of the kona storm: A subtropical cyclone. *J. Meteor.*, **9,** 24–35.

Smolarkiewicz, P. K., R. M. Rasmussen, and T. L. Clark, 1988: On the dynamics of Hawaiian cloud bands: Island forcing. *J. Atmos. Sci.*, **45,** 1872–1905.

Stewart, S., and S. W. Lyons, 1996: A WSR-88D radar view of Tropical Cyclone Ed. *Wea. Forecasting*, **11,** 115–135.

Ueyoshi, K., J. O. Roads, F. Fujioka, and D. E. Stevens, 1996: Numerical simulation of the Maui vortex in the trade winds. *J. Meteor. Soc. Japan*, **74,** 723–744.

Velden, C. S., 1996: Winds derived from geostationary satellite moisture channel observations: Applications and impact on numerical weather prediction. *Meteor. Atmos. Phys.*, **57,** 1–10.

Vincent, D. G., 1994: The South Pacific convergence zone (SPCZ): A review. *Mon. Wea. Rev.*, **122,** 1949–1970.

Wakimoto, R. M., and J. K. Lew, 1993: Observations of a Florida waterspout during CaPE. *Wea. Forecasting*, **8,** 412–423.

Wang, J. J., H.-M. H. Juang, Y. L. Chen, S. Businger, K. Kodama, and J. Partain, 1998: Application of the NCEP Regional Spectral Model to improve mesoscale weather forecasts in Hawaii. *Wea. Forecasting*, **13,** 560–575.

Whitfield, M. B., and S. W. Lyons, 1992: An upper-tropospheric low over Texas during summer. *Wea. Forecasting*, **7,** 89–106.

Worthley, L. E., 1967: Weather phenomena in Hawaii. Part I. Synoptic climatology of Hawaii. Hawaii Institute of Geophysics, University of Hawaii, 40 pp. [Available from Dept. of Meteorology, University of Hawaii, 2525 Correa Rd., Honolulu, HI 96822.]

Zhang, D.-L., and J. M. Fritsch, 1987: Numerical simulation of the meso-β scale structure and evolution of the 1977 Johnstown flood. Part II: Inertially stable warm-core vortex and the mesoscale convective complex. *J. Atmos. Sci.*, **44,** 2593–2612.

Zipser, E. J., 1969: The role of organized unsaturated convective downdrafts in the structure and rapid decay of an equatorial disturbance. *J. Appl. Meteor.*, **8,** 799–814.

——, 1977: Mesoscale and convective-scale downdrafts as distinct components of squall-line structure. *Mon. Wea. Rev.*, **105,** 1568–1589.

——, R. J. Meitín, and M. A. LeMone, 1981: Mesoscale motion fields associated with a slowly moving GATE convective band. *J. Atmos. Sci.*, **38,** 1725–1750.